Birkbeck
UNIVERSITY OF LONDON

BIROn - Birkbeck Institutional Research Online

Lai, Y.-J. and Pogge von Strandmann, Philip A.E. and Dohmen, R. and Takazawa, E. and Elliott, T. (2015) The influence of melt infiltration on the Li and Mg isotopic composition of the Horoman Peridotite Massif. Geochimica et Cosmochimica Acta 164 , pp. 318-332. ISSN 0016-7037.

Downloaded from: https://eprints.bbk.ac.uk/id/eprint/13144/

Usage Guidelines:
Please refer to usage guidelines at https://eprints.bbk.ac.uk/policies.html or alternatively contact lib-eprints@bbk.ac.uk.

The influence of melt infiltration on the Li and Mg isotopic composition of the Horoman Peridotite Massif

Yi-Jen Lai [a,b,*], Philip A.E. Pogge von Strandmann [a,c], Ralf Dohmen [a,d], Eiichi Takazawa [e,f], Tim Elliott [a]

[a] Bristol Isotope Group, School of Earth Science, University of Bristol, Bristol, UK

[b] Institute of Geochemistry and Petrology, ETH Zürich, Zürich, Switzerland

[c] Institute of Earth and Planetary Sciences, UCL and Birkbeck, University of London, London, UK

[d] Institute of Geology, Mineralogy and Geophysics Petrology, Ruhr-University Bochum, Germany

[e] Department of Geology, Faculty of Science, Niigata University, Japan

[f] Mantle and Continental Crust Drilling Research, Research and Development Center for Ocean Drilling Science, Japan Agency for Marine-Earth Science and Technology, Japan

* Corresponding author.

Email-address: yi-chen.lai@erdw.ethz.ch

Tel: +41 (0)446327713

Fax: +41 (0)446321376

Abstract

We have analysed the Li and Mg isotope ratios of a suite of samples from the Horoman peridotite massif. Our results show that most Li and all Mg isotopic compositions of the Horoman peridotites are constant over 100 metres of continuous outcrop, yielding values for pristine mantle of δ^{7}Li = 3.8 ± 1.4 ‰ (2SD, n = 9), δ^{25}Mg = -0.12 ± 0.02 ‰ and δ^{26}Mg = -

0.23 ± 0.04 ‰ (2SD, n = 17), in keeping with values for undisturbed mantle xenoliths. However, there are also some anomalously low δ^7Li values (-0.2 to 1.6 ‰), which coincide with locations that show enrichment of incompatible elements, indicative of the prior passage of small degree melts. We suggest Li diffused from the infiltrating melts with high [Li] into the low [Li] minerals and kinetically fractionated ^{7}Li/^{6}Li as a result. Continued diffusion after the melt flow had ceased would have resulted in the disappearance of this isotopically light signature in less than 15 Ma. In order to preserve this feature, the melt infiltration must have been a late stage event and the massif must have subsequently cooled over a maximum of ~0.3 Ma from peak temperature (950°C, assuming the melts are hydrous) to Li closure temperature (700°C), likely during emplacement. The constant δ^{26}Mg values of Horoman peridotites suggest that chemical potential gradients caused by melt infiltration were insufficient to drive associated δ^{26}Mg fractionation greater than our external precision of 0.03 ‰.

1. Introduction

Li isotopes should have value as a diagnostic tracer of plate recycling processes (see Elliott et al., 2004; Tomascak, 2004) owing to the large isotopic fractionations that occur in the hydrosphere and which are imparted to mafic oceanic crust (e.g. Chan et al. 1992). The recycling of isotopically heavy oceanic crust into the mantle is thought to generate heterogeneities seen in some mid-ocean ridge basalts (MORB) (Elliott et al., 2006; Tomascak et al., 2008) and ocean island basalts (OIB) (Ryan and Kyle, 2004; Nishio et al., 2005; Chan et al., 2009; Krienitz et al., 2012).

However, it has become clear that Li isotope ratios of mantle materials may have been perturbed by diffusive processes. The relative diffusivities of two isotopes of an element are mass-dependent according to a relationship commonly expressed in the form D_2/D_1 =

$(m_1/m_2)^{\beta}$, where D_1 and D_2 are the diffusivities of isotopes of masses m_1 and m_1 and β is an experimentally derived exponent. Richter et al. (2003 and 2014) reported the value of beta to be 0.215 for Li diffusion in silicate melts and 0.27 in pyroxene, indicating that ^{6}Li diffuses ~3-4 % faster than ^{7}Li. Experiments have shown that Li diffusion rates are very high in melts (Jambon and Semet, 1978; Lowry et al., 1981) and silicate minerals (Giletti and Shanahan, 1997; Coogan et al., 2005; Dohmen et al., 2010) compared to other cations, so diffusion-driven Li isotopic fractionation can occur over geologically short timescales. Variations in δ^{7}Li of up to 20-50 ‰ (virtually the entire terrestrial range) have been observed within individual igneous crystal grains that can be clearly related to diffusive control (Beck et al., 2006; Jeffcoate et al., 2007; Kaliwoda et al., 2008; Parkinson et al., 2007). Highly variable differences in δ^{7}Li between different bulk mineral analyses from xenoliths indicate isotopic disequilibrium likely driven by differential rates of Li diffusion (Jeffcoate et al., 2007; Rudnick and Ionov, 2007; Tang et al., 2007). Systematic changes in δ^{7}Li with macroscopic sampling position also implicate diffusional perturbation over a longer length-scale (Lundstrom et al., 2005; Teng et al., 2006).

To help assess the possible role of diffusion in influencing the Li isotopic composition of bulk xenoliths, Pogge von Strandmann et al. (2011) further measured Mg isotopes on the same samples. Mantle Mg isotope ratios should be uninfluenced by addition of recycled components, which are much poorer in MgO than peridotite, but Mg isotope ratios are sensitive to diffusion. Chemical diffusion experiments showed as much as 7 ‰ fractionation of ^{26}Mg/^{24}Mg, which is the second largest effect for a metal cation, after Li (Richter et al., 2003; Richter et al., 2008; Chopra et al., 2012). It has also been shown that Mg isotopic fractionation can result from thermal diffusion (Huang et al., 2010; Richter et al., 2008), although it has long been known that this process more significant in laboratory experiments than in nature (Bowen, 1921; Lesher and Walker, 1988; Walker et al., 1988). Recent work has

empirically suggested that such Soret diffusion of Mg is not an important geological phenomenon (Dauphas et al., 2010). Covariations of δ^{26}Mg and δ^{7}Li in some bulk xenoliths allowed Pogge von Strandmann et al. (2011) to identify the role of diffusion in perturbing the whole rock composition of these mantle samples. Such diffusive perturbation of bulk xenolith samples during entrainment and transport to the surface adds complexity to determining the appropriate δ^{7}Li and δ^{26}Mg for the mantle from small, lava-hosted xenoliths (Pogge von Strandmann et al. 2011).

In order to avoid material that has potentially experienced such late-stage disturbance, we have studied samples from the Horoman peridotite massif. Not only do alpine-type peridotites, such as Horoman, provide samples of the mantle that have not been entrained in melt but they provide an opportunity to examine the spatial variability of isotopic ratios on an outcrop scale (100m) as opposed to the decimetre scale of xenoliths. A drawback is that some alpine peridotites have been exposed at the Earth's surface for sufficient time to have experienced extensive weathering. The Horoman perdiotite is unusually fresh and thus provides an excellent opportunity to assess further the Li and Mg isotopic ratios of the upper mantle.

2. Geological background and samples

The Horoman peridotite massif has been emplaced at the southern end of the low-pressure, high-temperature Hidaka metamorphic belt in Japan. The massif is dominantly composed of repeating layered sequences of plagioclase lherzolite, lherzolite and harzburgite (Niida, 1974, 1984). It has been proposed that the Horoman peridotites are residues formed after partial melting of MORB source mantle (Takazawa et al., 1996a; Yoshikawa and Nakamura, 2000), possibly beneath an ultraslow palaeo-Pacific spreading ridge (Shimizu et al., 2006). Bulk peridotites with depleted light rare earth element (LREE) and ^{143}Nd/^{144}Nd

characteristics yield a Sm-Nd isochron age of 833 ± 78 Ma (Yoshikawa et al., 2000). Positively correlated $^{187}Re/^{188}Os$ and $^{187}Os/^{188}Os$ ratios of peridotite samples could be interpreted as an 'errorchron' of 0.91 ± 0.35 Ga lherzolite and mafic layers define an apparent Re-Os 'age' of 1.12 ± 0.24 Ga (Saal et al., 2001). Although Re-Os data do not define an isochron, Saal et al. (2001) suggested the age has geological meaning and the mafic layers and peridotites are related based on the age consistency of Re-Os and Sm-Nd systems. Malaviarachchi et al. (2008) have further suggested that melt depletion of the peridotites occurred at ~1 Ga ago based on both their $^{143}Nd/^{144}Nd$ and $^{177}Hf/^{176}Hf$ compositions. Thus there is now consensus that the layered peridotites formed after partial melting of a MORB source mantle ~0.8 - 1 Ga.

Some peridotites show evidence of later melt infiltration in the form of phlogopite bearing veins and cryptic metasomatism, which only results in LREE enrichment in clinopyroxenes (Takazawa et al., 1992). Takazawa et al. (1996b) proposed that host peridotites reacted with a LREE-enriched melt/fluid that had higher $^{87}Sr/^{86}Sr$ and lower $^{143}Nd/^{144}Nd$ isotopic ratios at the harzburgite and lherzolite boundary of the Bozu section (Takazawa et al., 1996b), the location investigated in this study. Yoshikawa and Nakamura (2000) inferred that the LREE-enriched, metasomatic agent is a fluid, possibly derived from the dehydration of the subducting slab based on generally elevated B/Nb and Pb/Ce ratios, although the differences in B/Nb and Pb/Ce ratios between metasomatised and non-metasomatised peridotites are not clear. Malaviarachchi et al. (2010) also proposed that the metasomatism agent for massive peridotites is fluid because of the enrichment in alkali elements (e.g. Rb). However, experimental results have demonstrated that both slab-derived fluid and melt could have high Rb concentrations, but only a melt could possibly have a high La concentration (Spandler et al., 2007). Hence, the metasomatic agent causing LREE (e,g. La) enrichment in the region is most likely to be melt. At the end of Miocene (~ 23 Ma), the

peridotites were metasomatised by fluid and formed phlogopite veins in the mantle wedge above the Hidaka subduction zone during emplacement based on Rb-Sr dating on samples with phlogopites (Yoshikawa et al., 1993; Yamamoto et al., 2010). During uplift and emplacement the peridotite was transformed from garnet- to spinel- to plagioclase-facies peridotites (Takazawa et al., 1996a; Ozawa, 2004).

Fifteen samples were selected for Li and Mg isotopic analyses from the layered 140 m Bozu section (Fig. 1). The petrology, P-T trajectory and geochemistry (e.g. major and trace element abundances, Sr and Nd isotope compositions) of this Bozu section have been well studied (Takazawa et al. 1992, 1996a, 1999 and 2000; Yoshikawa et al., 2000; Obata and Takazawa, 2004). These samples represent residues from a significant degree of partial melting (4 - 25%) ranging from fertile lherzolites (3-4 % Al_2O_3 and CaO) to depleted harzburgites (~0.5 % Al_2O_3 and CaO). The peridotites originally resided in the garnet stability field (~950 °C, ~1.9 GPa) before the ascent. We focus on determining Li and Mg isotope compositions of the whole rocks to determine bulk mantle composition. However, Li and Mg isotopic analyses of mineral separates of two samples (BZ-216 and BZ-250) are undertaken to examine inter-mineral isotopic fractionation. Most samples in this study show no signatures of the metasomatism identified in previous work (Takazawa et al., 1992; Takazawa et al., 1996a), and these should provide the best constraints for pristine mantle Li and Mg isotope compositions. A few selected samples show LREE enrichment (Fig. 2c), especially for the samples at around 22-23 m location, where percolation of a high-LREE concentration-, high $^{87}Sr/^{86}Sr$- and low $^{143}Nd/^{144}Nd$-melt was inferred (Takazawa et al., 1996b and 2000).

3. Methods

3.1 Chemical preparation of Li and Mg isotopic analysis

Rock powders were dissolved using a HF-HNO_3-$HClO_4$-HCl mixture. Mineral separates were first sonicated in acetone and 18 Mohm.cm (Milli-Q) H_2O before dissolution. Li and Mg isotopes were measured on aliquots of the same sample dissolutions. A sample containing ~10 ng Li was dried down and passed through Bio-Rad AG 50W - X12 (200-400 mesh) cation exchange resin using 0.2N HCl as an eluent to separate Li from matrix. Full details of the column procedures were reported in Marschall et al. (2007) and Pogge von Strandmann et al. (2011). Mg was separated from the matrix using the same resin and columns as for the Li chemistry described above, but using 2N HNO_3 as an eluent. Aliquots containing ~1 µg Mg were dried down and taken up in 2N HNO_3. Our two-step column procedure uses a first stage to separate Mg from the sample matrix, and a second column to further purify the Mg. Full details of the column procedures were reported in Pogge von Strandmann (2008) and further details about the combined Li and Mg techniques in Pogge von Strandmann et al. (2011).

3.2 Mass spectrometry

Li isotope ratios were measured on a Thermo Finnigan Neptune MC-ICP-MS (multi-collector inductively coupled plasma mass spectrometry) at the Bristol Isotope Group. The measurements followed the analysis method from Jeffcoate et al. (2004) and Pogge von Strandmann et al. (2011). Individual Li analyses comprised 10 static isotope measurements (each integration lasting 4.194 s) of ^{6}Li (L4) and ^{7}Li (H4), where L4 and H4 refer to the movable low-mass (L) and high-mass (H) Faraday cups. Uptake rates of ~50 µl min^{-1} for a 10 ng/g solution typically gave a total (^{6}Li + ^{7}Li) beam intensity of ~100 pA compared with an instrumental background of 0.4 pA. Each individual analysis comprises four measurements of each sample solution in the same session, with a typical precision of < 0.04 ‰ (2SD). In this study we made repeat analyses from different dissolutions and chemical purifications for most studies and the averages and 2SDs (standard deviation from the mean) of these duplicates are reported in Table 1 and 2. Li isotope values are reported in a δ^7Li notation

($\delta^7Li = (^7Li/^6Li_{sample}/ ^7Li/^6Li_{standard} - 1) \times 1000$) as ‰ variations of the $^7Li/^6Li$ ratio of the sample from that of the average of the bracketing standard, NIST SRM 8545 (L-SVEC) (Flesch et al., 1973), which was diluted to within ± 10% of the concentration of the samples. The Geological Survey of Japan (GSJ) JP-1 peridotite rock standard was analysed numerous times over the course of this study as an assessment of external reproducibility. JP-1 is an especially useful datum, since it is a peridotite sample of the Horoman. These measurements yielded an average $\delta^7L = +2.5 \pm 0.5$ ‰ (n = 14, 2SD), which is consistent with the values reported by Pogge von Strandmann et al. (2011) and Gao et al. (2012).

Magnesium isotope ratios were also measured on a Thermo Finnigan Neptune MC-ICP-MS at the University of Bristol coupled with an Apex Q introduction system. This suppresses CN^+ formation on ^{26}Mg, which is a problem using the Aridus desolvating introduction system, making it possible to analyse Mg isotopes at 'low' mass-resolution (~500M/ΔM) (Pogge von Strandmann et al., 2011). Mg solutions of 50 ng/g typically yield a beam intensity of ~100 pA on ^{24}Mg with a 50 µl/min uptake rate, compared to a background of 0.04 pA. A sample-standard bracketing procedure was adopted, relative to the Mg standard DSM-3 (Galy et al., 2003), which was diluted to within ± 10% of the concentration of the samples. All sample analyses are reported in the delta notation as ‰ deviations from this standard ($\delta^xMg = (^xMg/^{24}Mg_{sample}/ ^xMg/^{24}Mg_{standard} - 1) \times 1000$, where ^xMg is either ^{25}Mg or ^{26}Mg). Each sample was analysed three to five times during an analytical session, with each individual analysis separated by several hours. The averages and 2SDs of repeat analyses from different dissolutions and chemical purifications are listed in Table 1 and 2.

Our long term precision was determined by the Mg standard CAM-1, which yield a value of -2.61 ± 0.03 ‰ on $\delta^{26}Mg$ (2SD, n=24). We have previously documented the robustness of procedures against residual impurities after the separation chemistry and different methods of sample introduction (Pogge von Strandmann et al. 2011). We have further illustrated that an

198 intercept values obtained by a standard addition experiment between JP-1 and CAM-1 yield
199 values within error of the individual measurements (Pogge von Strandmann et al 2011). Over
200 the course of this study we measured two international rock standards, GSJ JP-1 and United
201 States Geological Survey (USGS) BHVO-2, as references and monitors of reproducibility for
202 silicate samples. For JP-1 we obtain a mean δ^{26}Mg = -0.23 ± 0.03 ‰ (2SD, n=17), which
203 compares well with other studies (-0.23 ± 0.03 ‰, Handler et al., 2009; -0.24 ± 0.05 ‰,
204 Pogge von Strandmann et al., 2011). Fewer repeat measurements of the basaltic standard,
205 BHVO-2, gave a mean a value of -0.25 ± 0.04 ‰ (n=3), which provides a comparable but
206 more precise measurement than reported in other studies (-0.16 ± 0.10 ‰, Bizzarro et al.,
207 2005; -0.14 ± 0.18 ‰, Weichert and Halliday, 2007; -0.24 ± 0.11 ‰, Pogge von Strandmann,
208 2008; -0.19 ± 0.07 ‰, Bizzarro et al., 2011; -0.24 ± 0.05 ‰, Pogge von Strandmann et al.,
209 2011).

210 **3.3 Determination of Li concentration by isotope dilution**

211 Li concentrations of the samples were determined by isotope dilution (ID) using 95%
212 enriched ^{6}Li spike, LISB (Li Isotope Spike in Bristol). The Li carbonate spike powder was
213 dissolved in Milli-Q H_2O and HNO_3 to make a stock solution in 2% HNO_3. The Li isotope
214 composition of the spike was determined by a double-filament technique using a Finnigan
215 Triton thermal ionization mass spectrometer (TIMS) at the University of Bristol, following
216 the method of Kasemann et al. (2005). The Li concentration of the spike was calibrated
217 against a gravimetric solution of the NIST Li isotope standard, SRM 8545 (L-SVEC).

218 Aliquots of rock powder containing about 15 ng of Li (about 10 mg of powder for
219 peridotites) were weighed and dissolved using our regular dissolution method for Li isotope
220 analysis (see 3.1). After complete dissolution, the sample was dried down and redissolved in
221 1 ml of 2% HNO_3. Then about 0.35 ml of the solution was transferred to another beaker and

spiked with 0.5 ml of 10 ng/g LISB to attain $(^{7}Li/^{6}Li)_{mixture}$ ratios of between 0.6 - 1.2. Solutions were diluted by a dilution factor (DF) >100 and measured on a Thermo Finnigan Element using wet plasma without Li separation chemistry. This simple methodology has been explored by Moriguti et al. (2004) who reported there is no matrix effect for solutions with DF > 97 using an ICP power setting >1.4 kW. However, we found the sampler cone became clogged using such matrix-rich solutions and caused the Li signal to drop quickly. Hence the ID samples were purified with a miniature version (0.25ml) of the Li separation procedure summarised above to remove most of the matrix.

A Thermo Finnigan Element ICP-MS was used for analytical measurements for Li spiked samples. We used a nebuliser with an uptake rate of 50 µl/min together with a quartz spray chamber. Normally 10 ng/g of Li solution yielded an intensity of ~ 240,000 cps on total Li. Instrumental blank was < 400 cps. A typical sequence involved L-SVEC, L-SVEC-LISB mixtures and spiked samples. Mass bias and drift were corrected by bracketed L-SVEC-LISB mixtures. The true $^{7}Li/^{6}Li$ ratios of the spiked samples were attained in relation to measured L-SVEC. GSJ JB-2 was analysed as an unknown and yielded [Li] = 7.59 ± 0.1 µg/g. The Li concentrations of the samples obtained by isotope dilution are listed in Table 1, where they are also compared with the concentrations acquired by peak height analysis on the Neptune.

4. Results

4. 1. Whole-rock analyses

Lithium and magnesium analyses are reported in Table 1. Li isotopic compositions and concentrations are presented in Fig. 2a, b with stratigraphic distance from the bottom of the sequence. The $\delta^{7}Li$ values of the Horoman peridotites range from -0.2 to 4.8 ‰ and the Li concentrations vary between 0.86 to 1.64 µg/g. The lowest $\delta^{7}Li$ values are evident at the harzburgite - lherzolite (~23 m) contact and within the plagioclase lherzolite (~90 m). These

246 δ^7Li troughs are coincident with elemental enrichments of Li (Fig. 2a, b; Fig. 3) and highly
247 incompatible elements (e.g. La, Sr; only La is shown in Fig. 2c), that mark metasomatic
248 pathways. There is some complexity in δ^7Li associated with [Li] gradients in the plagioclase
249 lherzolite zone, but there is an anomalously low value of δ^7Li associated with a spike in La
250 concentration at ~90 m. This feature is superimposed on an overall increase in Li, TiO_2 and
251 La concentrations away from the boundary with the spinel lherzolite (Fig. 2b-d), reflecting
252 differences in the amount of ancient melt depletion (see Section 2). As with the La
253 concentration spikes, δ^7Li changes sharply and for the higher resolution sampling at the base
254 of the section (~23 m), it can be seen that anomalously light Li isotope values return to
255 background over a 0.7 m scale (~23 m, see Fig 2a).

256 The δ^{26}Mg and Mg numbers of the bulk samples are presented in Fig. 4. The δ^{26}Mg
257 values vary from -0.19 to -0.27 ‰, which yield an average of -0.23 ± 0.04 ‰ (2SD). All
258 samples are thus essentially within analytical error of each other and the mean yields a value
259 consistent with assessments of primitive mantle and bulk silicate Earth values suggested by
260 other studies (Handler et al., 2009; Yang et al., 2009; Young et al., 2009; Bourdon et al., 2010;
261 Dauphas et al., 2010; Teng et al., 2010; Huang et al., 2011; Pogge von Strandmann et al.,
262 2011).

263 **4. 2. Mineral separates**

264 Lithium and magnesium isotope compositions of mineral separates from samples with
265 low δ^7Li samples (BZ-216 and BZ-250) were determined (Table 2 and Fig. 5). The olivine
266 separates in both samples show lower values of δ^7Li than in orthopyroxene separates. This
267 observation is similar to that reported in previous literature (Jeffcoate et al., 2007). The lower
268 δ^7Li values in olivines relative to orthopyroxenes have been explained by high-temperature
269 equilibrium isotope fractionation. It is worth noticing that the δ^7Li values of olivine and

orthopyroxene separates in this study are lower compared to the values obtained from Jeffcoate et al. (2007), but seem in keeping with the lower bulk δ^7Li values of BZ-216 and BZ-250 relative to fertile upper mantle values (~3.5 ‰, Jeffcoate et al., 2007; Pogge von Strandmann et al., 2011).

The analysed orthopyroxenes and olivines have identical Mg isotope compositions. However, the Mg isotope compositions in clinopyroxenes are all heavier than coexisting orthopyroxenes and olivines, which is in agreement with notions of equilibrium fractionation from other studies (Young et al., 2002; Wiechert and Halliday, 2007; Young et al., 2009; Chakrabarti and Jacobsen, 2010; Liu et al., 2011; Pogge von Strandmann et al., 2011) and theoretical calculations (Schauble, 2011; Huang et al. 2013). The calculated bulk δ^{25}Mg and δ^{26}Mg values based on mineral mode are consistent with measured bulk δ^{25}Mg and δ^{26}Mg values (Table 2).

5. Discussion

5. 1. Li and Mg isotope compositions of the mantle

5.1.1 Mg isotope composition of the upper mantle

Our analyses show that there are no systematic differences in δ^{26}Mg related to the variable degrees of partial melting (4 - 25 %) and local metasomatism experienced by the Horoman samples. The Bozu section represents a 0.4 – 0.9 km thick section with a modest palaeo thermal gradient of ~10 ± 8 ℃/km (Ozawa, 2004). Given such a minor temperature difference over a large diffusive length scale, the effects from thermally driven diffusion across the outcrop are not unsurprisingly insignificant. Moreover, there are also no obvious isotopic effects related to chemical differences at lithological boundaries that might be caused to diffusion driven by chemical potential gradients.

The Horoman peridotites analysed in this study, with no evidence of kinetic Mg

redistribution, suggest that the δ^{26}Mg value of the upper mantle is -0.23 ± 0.04 ‰ (2SD, n = 17). The value is consistent with previous comprehensive studies (Handler et al., 2009; Huang et al., 2009; Yang et al., 2009; Young et al., 2009; Bourdon et al., 2010; Dauphas et al., 2010; Teng et al., 2010; Bizzarro et al., 2011; Pogge von Strandmann et al., 2011) (Fig. 6), but inconsistent with two studies (Chakrabarti and Jacobsen, 2010; Wiechert and Halliday, 2007). The Chakrabarti and Jacobsen (2010) dataset shows a systematic offset, although the reason for this is unclear. The Mg isotope value of the peridotite standard, JP-1, in Weichert and Halliday (2007) is much heavier than in other studies (Handler et al., 2009; Pogge von Standmann et al., 2011). Therefore, it is not surprising that the Mg isotope composition of the Earth estimated in their study is slightly heavier than our value. It is also worth noting that the direct mantle samples, analysed in previous studies were peridotite xenoliths, which may be altered by diffusion and kinetic isotope fractionation due to interaction with the host melt (e.g. Pogge von Strandmann et al., 2011). The Mg isotopic composition of the terrestrial mantle is thus now further constrained by samples from a tectonically emplaced peridotite massif.

5.1.2 Li isotope composition of the upper mantle

The grey band in Fig. 2a shows the literature δ^7Li value (3.5 ± 0.5 ‰) of the fertile upper mantle as defined by Pogge von Strandmann et al. (2011) from mantle xenoliths. Except for the samples at the 22.2 - 22.9 m with high La concentrations and plagioclase lherzolite samples (see 5.2.1), the ‘normal’ samples have an average Li concentration of 1.1 ± 0.3 µg/g and an average δ^7Li of 3.8 ± 1.4 ‰, which is in agreement with Li concentration and δ^7Li values of the fertile mantle ([Li] = 1.6 ± 0.7; δ^7Li = 3.5 ± 0.5 ‰) given from xenolith samples (Pogge von Strandmann et al., 2011), reconstructions of the pristine mantle from peridotite mineral separates (δ^7Li ~3.5 ‰) estimated by Jeffcoate et al. (2007), and N-MORB (δ^7Li = 3.4 ± 1.4 ‰) given by (Tomascak et al., 2008). As for Mg, the very different

318 influences on the Li isotopic composition of the Horoman peridotite during its transport to the
319 surface, relative to mantle xenoliths or mantle derived melts, makes the consistency of our
320 new mantle measurements with previous values a reassuring indication of the reliability of
321 estimates of mantle δ^7Li.

322 **5. 2. Isotopically light Li in the Horoman peridotites**

323 Anomalously light Li isotope compositions are evident in some of the bulk peridotites
324 and minerals of the Horoman massif. Light Li isotope signatures in some mineral phases can
325 be explained as inter-mineral Li-redistribution during cooling (Jeffcoate et al., 2007; Ionov
326 and Seitz, 2008; Kaliwoda et al., 2008). However, closed-system Li-redistribution itself
327 would only cause transitory fractionations of Li isotopes between minerals and the bulk Li
328 isotopic compositions should remain unchanged.

329 The low δ^7Li in some bulk peridotites have been argued to be generated by kinetic
330 isotope fractionation due to Li diffusion from melt/host magma into entrained xenoliths
331 (Jeffcoate et al., 2007; Rudnick and Ionov, 2007; Tang et al., 2007). In contrast to xenoliths,
332 tectonically emplaced peridotites like the Horoman are much larger bodies and their
333 temperatures during transport to the surface cooler, which limits pervasive diffusive ingress
334 of Li into the peridotite during exhumation. However, in the metasomatised zones of the
335 Horoman massif there clearly has been previous ingress of externally sourced melts, which
336 can locally perturb Li isotopic compositions.

337 In Fig. 7 we sketch a conceptual scenario for how the anomalously light Li isotope
338 ratios in the metasomatised portions of the Horoman peridotite can be created. Existing
339 evidence of the nature of the percolating melts through the Horoman rocks suggests that they
340 were small degree melts, enriched in incompatible elements (e.g. light rare earth elements,
341 Fig. 2c) (Takahashi, 1992; Takazawa et al., 2000), as well as Li (Fig. 2b). These percolating
342 melts should thus generate a chemical potential gradient, particularly relative to the peridotite,

to drive diffusion of Li from melt into host peridotite (Fig. 7b). The light Li isotopic compositions preserved in the bulk samples such as BZ-216 indicate that the melt did not have enough time to isotopically equilibrate with the bulk rocks at this stage, as otherwise the bulk Li isotope composition of the peridotites should be the same Li isotopic composition as common mantle melts ~3.5 ‰. Thus the percolation of melt must have been short-lived. Admittedly, a percolating melt with an isotopically light Li isotopic composition might have been involved. Yet, a recent study of the δ^7Li in samples that span the main radiogenic, isotopic endmember compositions of the mantle show that such lavas have δ^7Li that varies little from an average value of ~3.4 ‰ and never lower than 2 ‰ (Krientiz et al 2012).

That the bulk rock affected by melt percolation (area 2h in Fig. 7c) retained its overall low δ^7Li signature and did not equilibrate with the surrounding rocks on a longer length scale, implies that closure temperature was reached before the low δ^7Li signature was dispersed across a greater volume of peridotite (Fig. 7c). In the following sections we examine quantitatively how Li isotope ratios and concentrations change at each stage (Fig. 7a-c), and the time scales required to account for the observations.

5.2.1 Generation of light δ^7Li and high Li concentrations by Li diffusion from melt veins to minerals in the host rock

Locations previously traversed by melt are marked with light Li isotope compositions and elevated La concentrations (22.2 - 22.9 m and 89.3 - 94.7 m) (Fig. 2a, c). An inferred, prior melt pathway is especially well characterised around 22.2 – 22.9 m given the systematic variations of LREE enrichments in clinopyroxene, high $^{87}Sr/^{86}Sr$ and low $^{143}Nd/^{144}Nd$ ratios of peridotites sampled here (Takazawa et al., 2000). We concentrate on modelling this location because it provides the most straightforward example of Li diffusion from transient melt channels into the host minerals (Fig. 7b). In contrast, the melt pathway at 89.3 - 94.7 m

367 in the plagioclase lherzolite, is more complicated, because it is superimposed on a pre-
368 existing [Li] gradient. As discussed above, the gradual decrease of TiO_2 contents and Li
369 concentrations from the plagioclase lherzolite to spinel lherzolite boundary indicates the
370 effects of variable prior melt depletion (Fig. 2b, d). These chemical gradients provide a
371 driving force for Li to diffuse from the high [Li] plagioclase lherzolite towards the low [Li]
372 spinel lherzolite. Over the ~ 1 Ga time since melt depletion (see section 2), this could lead to
373 low δ^7Li values along the boundary and higher δ^7Li in the middle of the plagioclase lherzolite
374 layer. Subsequently, the effects of melt-rock interaction as described above are superimposed
375 on the section between 89.3 - 94.7 m (Takazawa et al., 2000), locally raising [La] and
376 lowering δ^7Li. Although we argue that similar processes are at work in this late-stage, melt
377 percolation event in the plagioclase lherzolite field, the additional influences make it harder
378 to model.

379 To quantify how Li isotope ratios changed in the host rock with melt diffusion, we
380 applied a model similar to that used by Parkinson et al. (2007). We assume a spherical
381 geometry for the individual crystals with isotropic diffusion and the melt acting as an infinite
382 reservoir. The latter assumption defines a fixed concentration at the crystal rim estimated
383 from the Li content of a small degree mantle melt. Using degrees of melting from 0.1 – 2%
384 and mineral-melt partition coefficients (see Table 3), we calculate plausible values from
385 11.1 – 12.5 µg/g. The assumption of a constant melt [Li] may not be entirely valid for a
386 moderately incompatible element like Li, if the melt fraction is small, but if the melt is
387 continuously renewed during melt flow it may be a reasonable approximation. The melt-rock
388 interaction must occur at a sufficiently high temperature to allow melt percolation. The
389 temperature strongly controls the timescales calculated and so we model both a ‘dry’ melt at
390 1200°C and ‘wet’ melt at 950 °C. We assume that temperature remains constant over the
391 relatively short period of melt percolation. Assuming an initially homogenous crystal, the

appropriate equation (Crank, 1975) for the scenario is:

$$\frac{C-C_1}{C_0-C_1}=1+\frac{2a}{r\pi}\sum_{n=1}^{\infty}\frac{(-1)^n}{n}\sin\left(\frac{nr\pi}{a}\right)\exp\left(\frac{-Dn^2\pi^2t}{a^2}\right) \quad (1)$$

Equation 1 was used to simulate the concentration distribution of both Li isotopes in olivine and clinopyroxene using slightly different diffusion coefficients as given by $D_7/D_6 = (m_6/m_7)^{\beta}$ (Richter et al. 2014). The resulting kinetic isotope fractionation depends dominantly on four variables: 1) D, the diffusion coefficient of Li in minerals; 2) C_0, the constant Li concentration at the surface of the sphere; 3) C_1, the initial Li concentration in the mineral of interest; 4) β, the kinetic isotope fractionation parameter. ^{6}Li and ^{7}Li concentrations are evaluated at different distances (from $r = 0$ to $r = a$) in a spherical grain with time (t) and δ^7Li values are calculated based on the ^{6}Li and ^{7}Li. The concentration in the centre is given by the limit as r approaches 0, that is by

$$\frac{C-C_1}{C_0-C_1}=1+2\sum_{n=1}^{\infty}(-1)^n\exp\left(\frac{-Dn^2\pi^2t}{a^2}\right) \quad (2)$$

Table 3 summarises the input parameters used for the sphere diffusion model. The average Li concentration and Li isotope composition of a mineral at any given time is evaluated by integration. Assuming the Li concentration in a bulk mineral is C_b and the volume in a mineral is V, the Li concentration (C) is integrated in a sphere as following equations.

$$C_b=\frac{1}{V}\int_V C dV \quad (3)$$

$$C_b=\frac{1}{a^3}\int_0^a C(r)r^2dr \quad (4)$$

where C is the Li concentration in a sphere from equation (1), hence:

$$C_b = C_0 + \frac{6(C_0 - C_1)}{\pi^2} \sum_{n=1}^{\infty} \frac{1}{n^2} \exp\left(\frac{-Dn^2\pi^2 t}{a^2}\right) \quad (5)$$

Fig. 8 shows the integrated results of the spherical model for olivine compared to the mineral separate analysis from BZ-216. The curves show the evolving, model [Li] and δ^7Li of olivines as a function of time, for several different values of [Li] in the percolating melt resulting from different degrees of partial melting. Given the second stage, discussed below, will tend to increase δ^7Li, this first stage needs to generate olivines with δ^7Li at least as low as those observed. This is satisfied by durations of melt percolation ~1.5 (wet melt) and ~140 years (dry melt).

Given the much faster diffusivity of Li in clinopyroxene (Coogan et al., 2005) the successful solutions for olivine will generate clinopyroxene compositions that will have fully re-equilibrated with the melt in this melt buffered scenario. However, clinopyroxenes in BZ-216 have δ^7Li much lower than the model melt, similar to the isotopically light olivines (Table 2; Figure 5). We thus infer that lithium redistribution occurred to generate these low δ^7Li in clinopyroxene by exchange with olivine after the episode of melt percolation. We have not modelled this process, which is similar to that explored by Gao et al. (2011), but assume this mineral length scale process occurs rapidly during the out-crop scale diffusion of Li into the country rock, investigated below.

5. 2. Diffusion of Li from enriched-zone into country rock

The time necessary for Li diffusion from percolating melting into adjacent minerals and Li isotopic redistribution on the millimetre scale described above is geologically relatively short. However, the process of melt percolation leaves portions of mantle with elevated Li concentrations that will start to diffuse to surrounding peridotites with unperturbed

compositions while cooling (Fig 7c). We now examine how long this process will take and estimate the cooling duration of the Horoman peridotite. We define the thickness of the peridotite, that has been affected by melt percolation as 2h (cm) and assume this peridotite has an initial, uniform low δ^7Li value (~ 0.13 ‰), taken from the previous model (see 5.2.1) and high Li concentration (C_0, 1.44 μg/g from mass balance calculations based on Li compositions of olivine and clinopyroxene obtained from the model of the first stage and an estimate for Li composition of orthopyroxene). We can evaluate how the Li isotopic composition and concentration changes during diffusion from the enriched peridotite to its surroundings with time by using the diffusion model of a substance initially confined in the region 2h (Crank, 1975),

$$C(x,t) = \frac{1}{2} C_0 \left\{ \mathrm{erf}\, \frac{h-x}{2\sqrt{Dt}} + \mathrm{erf}\, \frac{h+x}{2\sqrt{Dt}} \right\} \quad (6)$$

Here we assume the initial thickness of the enriched peridotites is smaller than 70 cm, because the observed distance between the samples with the lowest δ^7Li values and normal mantle values is 70 cm (distance between sample BZ-216, BZ-201 and BZ-203 in Table 1). In this case the diffusion coefficient, *D*, is a bulk diffusion coefficient, where the individual diffusion properties of the multi-phase system including fast diffusion paths like interface and grain boundaries are averaged in an appropriate way. Such an approach is only justified in a certain time regime (Type A diffusion regime, e.g., Dohmen and Milke, 2010), in which a representative volume of rock can be homogenized effectively by diffusion. As we have argued before, the individual minerals of a rock specimen seem to reflect elemental and isotopic equilibrium and hence this time regime has been reached at some point.

Diffusion during geological cooling usually takes place over a wide range of temperatures, which change as a function of time, t. Thus, the diffusivity becomes a function

of time during cooling. This problem can be handled in a simple way by defining a new variable λ as $d\lambda = D(t)\,dt$ (e.g. Ganguly, 2002). Using this definition, the diffusion equation (Fick's 2nd law) can be transformed to the following partial differential equation:

$$\frac{\partial C}{\partial \lambda} = \frac{\partial^2 C}{\partial x^2}. \qquad (7)$$

The analytical solution of the given problem can be thus obtained by replacing in equation (6) the product Dt with λ, which is the only unknown for the fitting procedure. Based on the definition of λ, the thermal history of the rocks can be constrained by integration (Ganguly, 2002)

$$\lambda = \int_0^t D(t)dt \qquad (8)$$

The integration of $D(t)dt$ over the postulated T-t path must equal λ derived from modelling compositional gradient. Fig. 9 shows the modelling result from equation (6) with h = 35 cm (the modelling results cannot fit the data when h < 30 cm). The modelling curves provide the best fit for the data when λ is smaller than 1.39×10^{10} (μm^2). From the estimated value for λ we can now infer the cooling rate assuming a certain type of thermal history. For conductive cooling a good representation of the initial cooling phase is reciprocal cooling from the peak temperature, T_0 with a cooling rate constant, η, as follows:

$$\frac{1}{T} = \frac{1}{T_0} + \eta t \qquad (9)$$

It can be shown with equation (10) that the cooling rate constant can be calculated from λ, as follows (Ganguly 2002):

$$\eta = \frac{D(T_0)R}{\lambda Q} \qquad (10)$$

Where, $D(T_0)$ is the diffusion coefficient at peak temperature, Q is activation energy of diffusion and R is ideal gas constant. If we assume T_0 to be 1200℃ for Horoman peridotites in the Lower Zone (Ozawa, 2004), as might be appropriate if the percolating melts were anhydrous then the minimum cooling rate constant is inferred to be 1.51 x 10^{-15} $K^{-1}s^{-1}$, which for example implies that it takes maximum ~7300 years to cool from 1200 ℃ - 700 ℃. 700 ℃ was estimated to be the Li closure temperature of olivine according to Gao et al. (2011). We suggest that the cooling time reflects the rate of emplacement of the Horoman massif from a prior back-arc setting. A value of 7300 years seems a rapid time for a tectonically emplaced peridotite and so we also consider a much initial lower temperature, which implies that the infiltrating melts were hydrous and so could percolate at much lower temperatures. This scenario is compatible with the hydrous (phlogopite bearing) late mineral veins in the Horoman massif (Yoshikawa et al., 1993; Yamamoto et al., 2010). In this case the minimum cooling time from melt percolation to olivine closure is ~0.3 Ma.

5. 3. Comparison of Li diffusion model for a tectonically emplaced peridotite in the literature

The only previous numerical model to explain Li isotope compositions in a tectonically emplaced peridotite was reported by Lundstrom et al. (2005) for the Trinity Ophiolite. Lundstrom et al. (2005) reported troughs in δ^7Li in the harzburgitic margins of dunite channels though host lherzolites. Dunite channels have widely been inferred to record the prior paths of sub-ridge melt conduits paths of sub-ridge melt conduits and Lundtrom et al. (2005) suggested that the diffusion of Li from the higher [Li] melts to surrounding depleted mantle. In detail, melt extraction combined with diffusion was required to explain associated rare earth element and Li concentration profiles together with Li isotopic compositions. However, all these features were related to sub-ridge processes before the obduction of the

ophiolite. If we use the model described earlier (see 5.3) with recent diffusivity data in olivine and clinopyroxene (Coogan et al., 2005; Dohmen et al., 2010), the low δ^7Li signature generated by magmatic process at the original ridge setting could be homogenised in the 70 cm wide region studied by Lundstrom et al. (2005) within 0.3 Ma cooling duration (from 1200 °C to 700 °C). We suggest that this timescale to erase any primary Li isotopic signature is shorter than the moving a portion of melted mantle off axis and cooled to a temperature of 700°C. We therefore argue it is more likely that the systematic δ^7Li variation in Trinity ophiolite was generated in later event (e.g. emplacement), maybe as a result of changing chemical potential gradients in different mantle mineral phases during cooling (cf Gao et al., 2011).

6. Conclusions

The Li and Mg isotopes analysed in peridotites from the Horoman Peridotite Massif provide us with better constraints on the Mg and Li isotope compositions of the primitive mantle, and diffusion processes at high temperature. The identical Mg isotope compositions in the Horoman peridotites, which cover fertile plagioclase lherzolites to depleted harzburgites, suggests that the Mg isotope composition of the primitive upper mantle is δ^{25}Mg = -0.12 ‰ ± 0.02 ‰ and δ^{26}Mg = -0.23 ‰ ± 0.04 ‰ (2SD, n = 17). The average δ^7Li values of the samples without Li and La enrichment in this study are consistent with the literature data and give an average Li concentration of 1.1 ± 0.3 μg/g and an average δ^7Li of 3.8 ± 1.4 ‰ (2SD, n = 9)

The low δ^7Li values in bulk peridotites and mineral separates indicate diffusion processes are involved in generating low δ^7Li values in whole rocks. Results from diffusion in a sphere model show that it likely took 1.5 years and 140 years to drive the δ^7Li value of olivine ~3 ‰ lower at 1200 °C and 950 °C respectively, once the melt was removed from

around the minerals, whereas the clinopyroxene had been in equilibrium with the melts given the much faster diffusivity of Li in clinopyroxene. The disequilibrium between olivine and clinopyroxene caused Li to redistribute itself between minerals. The low δ^7Li values in melt-influenced bulk peridotites was preserved implying maximum ~0.3 Ma for the cooling duration from peak temperature (950 °C) to Li closure temperature (700 °C). This combined analytical and modelling approach also demonstrates that it is possible to tease out multiple metasomatic processes from the Li isotope data, and that conceivably this method can be used to study emplacement and metasomatism processes in detail. Li provides a novel means of estimating the timing and duration of these events. It also reiterates that the previously heralded recycling tracer, Li, is complicated by diffusion.

Acknowledgements

Simon Kohn and Ian Parkinson are thanked for discussion and comments on early draft. Chris Coath is thanked for for the sweet running of the MC-ICP-MS and helping improve the technique for Mg isotope analysis. Simone Kasemann is thanked for demonstrating Li isotope measurement on TIMS. Y.-J. Lai was supported by ORSAS (Overseas Research Students Awards Scheme) from the British council and postgraduate scholarship from the School of Earth Sciences at the University of Bristol. PPvS and part of this work was supported by NERC grant NE/C510983/1. Paul Tomascak and two anonymous reviewers are thanked for their helpful comments.

References

Beck P., Chaussidon M., Barrat J.A., Gillet P. and Bohn M. (2006) Diffusion induced Li isotopic fractionation during the cooling of magmatic rocks: The case of pyroxene phenocrysts from nakhlite meteorites. *Geochim. Cosmochim. Acta* **70**, 4813-4825.

Bizzarro M., Paton C., Larsen K., Schiller M., Trinquier A. and Ulfbeck D. (2011) High-precision Mg-isotope measurements of terrestrial and extraterrestrial material by HR-MC-ICPMS-implications for the relative and absolute Mg-isotope composition of the bulk silicate Earth. *J. Anal Atom. Spectrom.* **26**, 565-577.

Bourdon B., Tipper E.T., Fitoussi C. and Stracke A. (2010) Chondritic Mg isotope composition of the Earth. *Geochim. Cosmochim. Acta* **74**, 5069-5083.

Bowen N.L. (1921) Diffusion in silicate melts. *J. Geol.* **29(4)**, 295-317

Brenan J.M., Neroda E., Lundstrom C.C., Shaw H.F., Ryerson F.J. and Phinney D.L. (1998) Behaviour of boron, beryllium, and lithium during melting and crystallization: Constraints from mineral-melt partitioning experiments. *Geochim. Cosmochim. Acta* **62**, 2129-2141.

Chakrabarti R. and Jacobsen S.B. (2010) The isotopic composition of magnesium in the inner Solar System. *Earth Planet. Sc. Lett.* **293**, 349-358.

Chan L.H., Lassiter J.C., Hauri E.H., Hart S.R. and Blusztajn J. (2009) Lithium isotope systematics of lavas from the Cook-Austral Islands: Constraints on the origin of HIMU mantle. *Earth Planet. Sc. Lett.* **277**, 433-442.

Chopra R., Richter F.M., Watson E.B. and Scullard C.R. (2012) Magnesium isotope fractionation by chemical diffusion in natural settings and in laboratory analogues. *Geochim. Cosmochim. Acta* **88**, 1-18.

Coogan L.A., Kasemann S.A. and Chakraborty S. (2005) Rates of hydrothermal cooling of new oceanic upper crust derived from lithium-geospeedometry. *Earth Planet. Sc. Lett.* **240**, 415-424.

Dauphas N., Teng F.Z. and Arndt N.T. (2010) Magnesium and iron isotopes in 2.7 Ga Alexo komatiites: Mantle signatures, no evidence for Soret diffusion, and identification of diffusive transport in zoned olivine. *Geochim. Cosmochim. Acta* **74**, 3274-3291.

Dohmen R., Kasemann S.A., Coogan, L. and Chakraborty S. (2010) Diffusion of Li in olivine. Part I: Experimental observations and a multi species diffusion model. *Geochim. Cosmochim. Acta* **74**, 274-292.

Dohmen R. and Milke R. (2010) Diffusion in Polycrystalline Materials Grain Boundaries, Mathematical Models, and Experimental Data, in: Zhang, Y.X., Cherniak, D.J. (Eds.), *Diffusion in Minerals and Melts* 921-970.

Elliott T., Jeffcoate A. and Bouman C. (2004) The terrestrial Li isotope cycle: light-weight constraints on mantle convection. *Earth Planet. Sc. Lett.* **220**, 231-245.

Elliott T., Thomas A., Jeffcoate A. and Niu Y.L. (2006) Lithium isotope evidence for subduction-enriched mantle in the source of mid-ocean-ridge basalts. *Nature* **443**, 565-568.

Flesch G.D., Anderson Jr. A.R. and Svec H.J. (1973) A secondary isotopic standard for $^{6}Li/^{7}Li$ determinations. *Int. J. Mass Ion Process.* **12**, 265-272.

Gallagher K. and Elliott T. (2009) Fractionation of lithium isotopes in magmatic systems as a natural consequence of cooling. *Earth Planet. Sc. Lett.* **278**, 286-296.

Galy A., Yoffe O., Janney P.E., Williams R.W., Cloquet C., Alard O., Halicz L., Wadhwa M., Hutcheon I.D., Ramon E. and Carignan J. (2003) Magnesium isotope heterogeneity of the isotopic standard SRM980 and new reference materials for magnesium-isotope-ratio measurements. *J. Anal. Atom. Spectrom.* **18**, 1352-1356.

Ganguly J. (2002) Diffusion kinetics in minerals: Principles and applications to tectono-metamorphic processes. *EMU Notes in Mineralogy* **4**, 271-309.

Gao Y.J., Snow J.E., Casey J.F. and Yu J.B. (2011) Cooling-induced fractionation of mantle Li isotopes from the ultraslow-spreading Gakkel Ridge. *Earth Planet. Sc. Lett.* **301**, 231-240.

Giletti B.J. and Shanahan T.M. (1997) Alkali diffusion in plagioclase feldspar. *Chem. Geol.* **139**, 3-20.

Handler M.R., Baker J.A., Schiller M., Bennett V.C. and Yaxley G.M. (2009) Magnesium stable isotope composition of Earth's upper mantle. *Earth Planet. Sc. Lett.* **282**, 306-313.

Huang F., Chakraborty P., Lundstrom C.C., Holmden C., Glessner J.J.G., Kieffer S.W. and Lesher C.E. (2010) Isotope fractionation in silicate melts by thermal diffusion. *Nature* **464**, 396-400.

Huang F., Glessner J., Ianno A., Lundstrom C. and Zhang Z.F. (2009) Magnesium isotopic composition of igneous rock standards measured by MC-ICP-MS. *Chem Geol* **268**, 15-23.

Huang F., Zhang Z., Lundstrom C.C. and Zhi X. (2011) Iron and magnesium isotopic compositions of peridotite xenoliths from Eastern China. *Geochim. Cosmochim. Acta* **75**, 3318-3334.

Huang F., Chen L., Wu Z., Wang W. (2013) First-principles calculations of equilibrium Mg isotope fractionations betwee garnet, clinopyroxene, orthopyroxene, and olivine: Implications for Mg isotope thermometry. *Earth Planet. Sc. Lett.* **367**, 61-70.

Ionov D.A. and Seitz H.M. (2008) Lithium abundances and isotopic compositions in mantle xenoliths from subduction and intra-plate settings: Mantle sources vs. eruption histories. *Earth Planet. Sc. Lett.* **266**, 316-331.

Jambon A. and Semet M.P. (1978) Lithium diffusion in silicate glasses of albite, orthoclase, and obsidian composition: an ion-microprobe determination. *Earth Planet. Sc. Lett.* **37**, 445-450.

Jeffcoate A.B., Elliott T., Kasemann S.A., Ionov D., Cooper K. and Brooker R. (2007) Li isotope fractionation in peridotites and mafic melts. *Geochim. Cosmochim. Acta* **71**, 202-218.

Jeffcoate A.B., Elliott T., Thomas A. and Bouman C. (2004) Precise, small sample size determinations of lithium isotopic compositions of geological reference materials and modern seawater by MC-ICP-MS. *Geostand. Geoanal. Res.* **28**, 161-172.

Kaliwoda M., Ludwig T. and Altherr R. (2008) A new SIMS study of Li, Be, B and δ^7Li in mantle xenoliths from Harrat Uwayrid (Saudi Arabia). *Lithos* **106**, 261-279.

Kasemann S.A., Jeffcoate A.B. and Elliott T. (2005) Lithium isotope composition of basalt glass reference material. *Anal. Chem.* **77**, 5251-5257.

Kil Y. (2010) Lithium isotopic disequilibrium of minerals in the spinel lherzolite xenoliths from Boeun, Korea. *J. of Geochem. Explor.* **107**, 56-62.

Krienitz M.S., Garbe-Schonberg C.D., Romer R.L., Meixner A., Haase K.M. and Stroncik N.A. (2012) Lithium isotope variations in ocean island basalts - implications for the development of mantle heterogeneity. *J. Petrol.* **53**, 2333-2347.

Lesher C.E. and Walker D. (1988) Cumulate maturation and melt migration in a temperature-gradient. *J. Geophys. Res.-Solid.* **93**, 10295-10311.

Li W.Y., Teng F.Z., Xiao Y.L. and Huang J.A. (2011) High-temperature inter-mineral magnesium isotope fractionation in eclogite from the Dabie orogen, China. *Earth Planet. Sc. Lett.* **304**, 224-230.

Liu S.A., Teng F.Z., Yang W., Wu F.Y. (2011) High-temperature inter-mineral magnesium isotope fractionation in mantle xenoliths from the North China craton. *Earth Planet. Sc. Lett.* **308**, 131-140.

Lowry R.K., Reed S.J.B., Nolan J., Henderson P. and Long J.V.P. (1981) Lithium tracer-diffusion in an alkali-basaltic melt - an ion-microprobe determination. *Earth Planet. Sc. Lett.* **53**, 36-40.

Lundstrom C.C., Chaussidon M., Hsui A.T., Kelemen P. and Zimmerman M. (2005) Observations of Li isotopic variations in the Trinity Ophiolite: Evidence for isotopic fractionation by diffusion during mantle melting. *Geochim. Cosmochim. Acta* **69**, 735-751.

Magna T., Ionov D.A., Oberli F. and Wiechert U. (2008) Links between mantle metasomatism and lithium isotopes: Evidence from glass-bearing and cryptically metasomatized xenoliths from Mongolia. *Earth Planet. Sc. Lett.* **276**, 214-222.

Magna T., Wiechert U. and Halliday A.N. (2006) New constraints on the lithium isotope compositions of the Moon and terrestrial planets. *Earth Planet. Sc. Lett.* **243**, 336-353.

Malaviarachchi S.P.K., Makishima A. and Nakamura E. (2010) Melt-peridotite reactions and fluid metasomatism in the upper mantle, revealed from the geochemistry of peridotite and gabbro from the Horoman Peridotite Massif, Japan. *J. of Petrol.* **51**, 1417-1445.

Malaviarachchi S.P.K., Makishima A., Tanimoto M., Kuritani T. and Nakamura E. (2008) Highly unradiogenic lead isotope ratios from the Horoman peridotite in Japan. *Nat. Geosci.* **1**, 859-863.

Marschall H.R., Pogge von Strandmann P.A.E., Seitz H.M., Elliott T. and Niu Y.L. (2007) The lithium isotopic composition of orogenic eclogites and deep subducted slabs. *Earth Planet. Sc. Lett.* **262**, 563-580.

McDonough W.F. and Sun S.S. (1995) The composition of the Earth. *Chem. Geol.* **120**, 223-

253.

Niida K. (1974) Structure of the Horoman ultramafic massif of the Hidaka metamorphic belt in Hokkaido, Japan. *J. Geol. Soc. Jpn.* **80**, 31-44.

Niida K. (1984) Petrology of the Horoman ultramafic rocks in the Hidaka metamorphic belt, Hokkaido, Japan. *J. Fac. Sci. Hokkaido Uni. IV* **21**, 197-250.

Nishio Y., Nakai S., Kogiso T. and Barsczus H.G. (2005) Lithium, strontium, and neodymium isotopic compositions of oceanic island basalts in the Polynesian region: constraints on a Polynesian HIMU origin. Geochemical Journal 39, 91-103.

Obata M. and Takazawa E. (2004) Compositional continuity and discontinuity in the Horoman peridotite, Japan, and its implication for melt extraction processes in partially molten upper mantle. *J. Petrol.* **45**, 223-234.

Ottolini L., Laporte D., Raffone N., Devidal J.-L. and Le Fevre B. (2009) New experimental determination of Li and B partition coefficients during upper mantle partial melting. *Contrib. Mineral. and Petr.* **157**, 313-325.

Ozawa K. (2004) Thermal history of the Horoman Peridotite Complex: A record of thermal perturbation in the lithospheric mantle. *J. Petrol.* **45**, 253-273.

Parkinson I.J., Hammond S.J., James R.H. and Rogers N.W. (2007) High-temperature lithium isotope fractionation: Insights from lithium isotope diffusion in magmatic systems. *Earth Planet. Sc. Lett.* **257**, 609-621.

Pearson D.G., Canil D. and Shirey S.B. (2004). Mantle samples included in volcanic rocks: xenoliths and diamonds. *In: Treatise on Geochemistry.* Holland, H.D. and Turrekian, K.K. (Editors), Elsevier, Amsterdam, The Netherlands. **2**, 171-275.

Pogge von Strandmann, P. A. E. (2008) Precise magnesium isotope measurements in core top planktic and benthic foraminifera. *Geochem. Geophys. Geosyst.* **9**, Q12015. doi:10.1029/2008GC002209.

Pogge von Strandmann P.A.E., Elliott T., Marschall H.R., Coath C., Lai Y.-J., Jeffcoate A.B. and Ionov D.A. (2011) Variations of Li and Mg isotope ratios in bulk chondrites and mantle xenoliths. *Geochim. Cosmochim. Acta* **75**, 5247-5268.

Richter F., Watson B., Chaussidon M., Mendybaev R. and Ruscitto D. (2014) Lithium isotope fractionation by diffusion in minerals. Part 1: Pyroxenes. *Geochim. Cosmochim. Acta* **126**, 352-370.

Richter F.M., Davis A.M., DePaolo D.J. and Watson E.B. (2003) Isotope fractionation by chemical diffusion between molten basalt and rhyolite. *Geochim. Cosmochim. Acta* **67**, 3905-3923.

Richter F.M., Liang Y. and Davis A.M. (1999) Isotope fractionation by diffusion in molten oxides. *Geochim. Cosmochim. Acta* **63**, 2853-2861.

Richter F.M., Watson E.B., Mendybaev R.A., Teng F.Z. and Janney P.E. (2008) Magnesium isotope fractionation in silicate melts by chemical and thermal diffusion. *Geochim.*

Cosmochim. Acta **72**, 206-220.

Rudnick R.L. and Ionov D.A. (2007) Lithium elemental and isotopic disequilibrium in minerals from peridotite xenoliths from far-east Russia: Product of recent melt/fluid-rock reaction. *Earth Planet. Sc. Lett.* **256**, 278-293.

Rudnick R.L., Tomascak P.B., Njo H.B. and Gardner L.R. (2004) Extreme lithium isotopic fractionation during continental weathering revealed in saprolites from South Carolina. *Chem. Geol.* **212**, 45-57.

Ryan J.G. and Kyle P.R. (2004) Lithium abundance and lithium isotope variations in mantle sources: insights from intraplate volcanic rocks from Ross Island and Marie Byrd Land (Antarctica) and other oceanic islands. *Chem. Geol.* **212**, 125-142.

Saal A.E., Takazawa E., Frey F.A., Shimizu N. and Hart S.R. (2001) Re-Os isotopes in the Horoman peridotite: Evidence for refertilization? *J. Petrol.* **42**, 25-37.

Schauble E.A. (2011) First-principles estimates of equilibrium magnesium isotope fractionation in silicate, oxide, carbonate and hexaaquamagnesium(2+) crystals. *Geochim. Cosmochim. Acta* **75**, 844-869.

Seitz H.M., Brey G.P., Lahaye Y., Durali S. and Weyer S. (2004) Lithium isotopic signatures of peridotite xenoliths and isotopic fractionation at high temperature between olivine and pyroxenes. *Chem. Geol.* **212**, 163-177.

Seitz H.M. and Woodland A.B. (2000) The distribution of lithium in peridotitic and pyroxenitic mantle lithologies - an indicator of magmatic and metasomatic processes. *Chem. Geol.* **166**, 47-64.

Shimizu N., Warren J.M., Frey F.A. and Takazawa E. (2006) The Horoman Peridotite Massif: an example of ancient ultraslow-spreading ridge abyssal peridotites? *EOS Trans. 87, Amer. Geophys. Union, Fall Meeting 2006*, **abstract**, V2012C2007S.

Spandler C., Mavrogenes J. and Hermann J. (2007) Experimental constraints on element mobility from subducted sediments using high-P synthetic fluid/melt inclusions. *Chem. Geol.* **239**, 228-249.

Su B.-X., Zhang H.-F., Deloule E., Sakyi P.A., Xiao Y., Tang Y.-J., Hu Y., Ying J.-F. and Liu P.-P. (2012) Extremely high Li and low δ^7Li signatures in the lithospheric mantle. *Chem. Geol.* **292**, 149-157.

Takahashi N. (1992) Evidence for melt segregation towards fractures in the Horoman Mantle Peridotite Complex. *Nature* **359**, 52-55.

Takazawa E., Frey F.A., Shimizu N., Obata M. and Bodinier J.L. (1992) Geochemical Evidence for Melt Migration and Reaction in the Upper Mantle. *Nature* **359**, 55-58.

Takazawa E., Frey, F., Shimizu, N. and Obata, M. (1996a) Evolution of the Horoman Peridotite (Hokkaido, Japan): Implications from pyroxene compositions. *Chem. Geol*. **134**, 3-26.

Takazawa, E. (1996b) *Geodynamic evolution of the Horoman peridotite, Japan: Geochemical study of asthenospheric and lithospheric processes*. Ph.D. dissertstion, Mass. Inst. Tech.

Takazawa E., Frey F.A., Shimizu N., Saal A. and Obata M. (1999) Polybaric petrogenesis of mafic layers in the Horoman peridotite complex, Japan. *J. Petrol.* **40**, 1827-1851.

Takazawa E., Frey F.A., Shimizu N. and Obata M. (2000) Whole rock compositional variations in an upper mantle peridotite (Horoman, Hokkaido, Japan): Are they consistent with a partial melting process? *Geochim. Cosmochim. Acta* **64**, 695-716.

Tang Y.J., Zhang H.F., Nakamura E., Moriguti T., Kobayashi K. and Ying J.F. (2007) Lithium isotope systematics of peridotite xenoliths from Hannuoba, North China Craton: implications for melt-rock interaction in the considerably thinned lithospheric mantle. *Geochim. Cosmchim. Acta.* **71**, 4327-4341.

Teng F.Z., Li W.Y., Ke S., Marty B., Dauphas N., Huang S.C., Wu F.Y. and Pourmand, A. (2010) Magnesium isotopic composition of the Earth and chondrites. *Geochim. Cosmochim. Acta* **74**, 4150-4166.

Teng F.Z., McDonough W.F., Rudnick R.L. and Walker R.J. (2006) Diffusion-driven extreme lithium isotopic fractionation in country rocks of the Tin Mountain pegmatite. *Earth Planet. Sc. Lett.* **243**, 701-710.

Tomascak P.B. (2004) Developments in the understanding and application of lithium isotopes in the earth and planetary sciences. *Rev. Mineral Geochem.* **55**: 153-195.

Tomascak P.B., Langmuir C.H., le Roux P.J. and Shirey S.B. (2008) Lithium isotopes in global mid-ocean ridge basalts. *Geochim. Cosmochim. Acta* **72**, 1626-1637.

Walker D., Jurewicz S. and Watson E.B. (1988) Adcumulus dunite growth in a laboratory thermal-gradient. *Contrib. Mineral. and Petr.* **99**, 306-319.

Wiechert U. and Halliday A.N. (2007) Non-chondritic magnesium and the origins of the inner terrestrial planets. *Earth Planet. Sc. Lett.* **256**, 360-371.

Xu R., Liu Y.S., Tong X.R., Hu Z.C., Zong K.Q. and Gao S. (2013) In-situ trace elements and Li and Sr isotopes in peridotite xenoliths from Kuandian, North China Craton: Insights into Pacific slab subduction-related mantle modification. *Chem. Geol.* **354**, 107-123.

Yakob J.L., Feineman M.D., Deane J.A., Jr. Eggler D.H. and Penniston-Dorland S.C. (2012) Lithium partitioning between olivine and diopside at upper mantle conditions: An experimental study. *Earth Planet. Sc. Lett.* **329**, 11-21.

Yamamoto H., Nakamori N., Terabayashi M., Rehman H.U., Ishikawa M., Kaneko Y. and Matsui T. (2010) Subhorizontal tectonic framework of the Horoman peridotite complex and enveloping crustal rocks, south-central Hokkaido, Japan. *Isl. Arc* **19**, 458-469.

Yang W., Teng F.Z. and Zhang H.F. (2009) Chondritic magnesium isotopic composition of the terrestrial mantle: A case study of peridotite xenoliths from the North China craton. *Earth Planet. Sc. Lett.* **288**, 475-482.

Yoshikawa M. and Nakamura E. (2000) Geochemical evolution of the Horoman peridotite complex: Implications for melt extraction, metasomatism, and compositional layering in the mantle. *J. Geophys. Res.-Solid* **105**, 2879-2901.

Yoshikawa M., Nakamura E. and Takahashi N. (1993) Rb-Sr isotope systematics in a phlogopite-bearing spinel lherzolite and its implications for age and origin of metasomatism in the Horoman peridotite complex, Hokkaido, Japan. *J. Mineral. Petrol. Econ. Geol.* **88**, 121-130.

Young E.D., Galy A. and Nagahara H. (2002) Kinetic and equilibrium mass-dependent isotope fractionation laws in nature and their geochemical and cosmochemical significance. *Geochim. Cosmochim. Acta* **66**, 1095-1104.

Young E.D., Tonui E., Manning C.E., Schauble E. and Macris C.A. (2009) Spinel-olivine magnesium isotope thermometry in the mantle and implications for the Mg isotopic composition of Earth. *Earth Planet. Sc. Lett.* **288**, 524-533.

Zhang H.F., Deloule E., Tang Y.J. and Ying J.F. (2010) Melt/rock interaction in remains of refertilized Archean lithospheric mantle in Jiaodong Peninsula, North China Craton: Li isotopic evidence. *Contrib. Mineral. and Petr.* **160**, 261-277.

Figure Captions

Figure 1. Sample localities along the Bozu straigraphic section in the Horoman peridotite modified from Takazawa et al. (1999, 2000). The Bozu section has a layered sequence typical of a peridotite mantle section and grades from plagioclase lherzolite through lherzolite to harzburgites. The N-type and E-type plagioclase lherzolites have different petrology and chemical composition. The N-type plagioclase lherzolites have relatively high CaO, Na_2O_3, Al_2O_3, TiO_2, heavy rare earth element (HREE) contents and low Mg number. The E-type plagioclase lherzolite, on the other hand, is enriched in light rare earth element (LREE).

Figure 2. (a) δ^7Li (b) Li abundance (c) La concentration (Takazawa et al., 2000) normalised to CI chondrite (McDounough and Sun, 1995) (d) TiO_2 contents normalised to the primitive mantle (Pearson et al., 2004) versus distances for the samples as a function of stratigraphic distances from the contact between mafic layer and dunite. The dashed lines represent the lithological boundaries. The 2SD represents external reproducibility of peridotite standard JP-1. The grey bend shows the range of δ^7Li value in the fertile mantle based on peridotite xenoliths (Pogge von Strandmann et al., 2011).

Figure 3. Lithium isotope compositions versus lithium concentrations for peridotite samples from Horoman. The error bars represent 2SD.

Figure 4. (a) The results of Mg isotopic compositions from this study and (b) Mg# (Takazawa et al., 2000) for the Horoman peridotite complex plotted as a function of stratigraphic distance. The 2SD represents external reproducibility of peridotite standard JP-1.

Figure 5. Li and Mg isotopic compositions of minerals in sample BZ-216 and BZ-250. The error bars represent external reproducibility of peridotite standard JP-1.

Figure 6. Comparison of the Mg isotope composition of the upper mantle obtained from this study and the literature.

Figure 7. An illustration of the three-stage diffusion processes during/after melts percolate into the minerals (see text for details). (a) Initial condition of the mantle. (b) Li diffusion from a sealed percolating melt into minerals in the region of thickness 2h. (c) Li redistribution between minerals after the melt is gone. (d) Li diffuses from area 2h to surrounding peridotites.

Figure 8. Modelled results of Li isotopic ratios and Li concentrations in olivine after different times and for different concentrations of percolating melts for diffusion at 950 ℃ and 1200 ℃ in a sphere model. The initial composition of olivine is shown at t = 0, which are calculated based on equilibrium isotope fractionation in the minerals at high temperature (Jeffcoate et al., 2007; Seitz et al., 2004). The compositions of the olivine equilibrated with the infiltrating melts are shown at t = 25 and 1000 (years) at 1200℃ and 950℃ respectively. The Li concentrations of the melts are calculated based on 0.1, 1 and 2 % degree of partial melting from a primitive mantle source respectively. Li diffusivities in olivine are from Dohmen et al. (2010) and Coogan et al. (2005). β is 0.27 from Richter et al. (2014). The parameters used for diffusion in a sphere model are listed in Table 3. The Li composition of measured olivine in sample BZ-216 is

also shown to compare with the modelled results.

Figure 9. Evaluation the second stage (a) Li isotopic ratios and (b) Li concentration variation using non-isothermal diffusion models using Equation (6) to estimate the best fit to measured data and to obtain λ. The area where melt infiltrated (enriched zone) is shown as "2h". The initial bulk composition of the peridotites at the enriched zone is obtained from the first stage model (see Figure 8). The initial composition of the country rock is shown as the gray line, which is calculated by averaging the compositions of the country rocks on the left- and right-hand side of the enriched zone ([Li] = 1.1 μg/g, δ^7Li = 3.6 ‰) excluding the plagioclase lherzolites. The modelled curves fit our measured data when the λ is smaller than 1.39×10^{10}.

Table 1

Table 1 Lithium concentrations and Li and Mg isotopic compositions in mantle peridotites from Horoman, Japan. The numbers of analytical sessions is represented by "n". Each analytical session contains 4 measurements. The 2SD represents the 'external' reproducibility instead of repeats measured in a single analytical session (4 measurements). The 2SD is not shown when the measurement of the sample was obtained from one single analytical session.

Sample ID	Height (m)	Rock type	Dissolutions	Chemistry	n	δ^7Li (‰)	2SD	[Li] [a] (μg/g)	2SD	[Li] [b] (μg/g)	2SD	Dissolutions	Chemistry	n	δ^{26}Mg (‰)	2SD	δ^{25}Mg (‰)	2SD	MgO (wt %)	Mg #	La [c] (ng/g)
BZ-125L	4.1	Harzburgite	1	2	2	2.3	0.3	1.01	0.03	1.11	0.16	1	1	1	-0.22		-0.12		45.72	0.914	5.00
BZ-116	9.1	Harzburgite	2	3	3	4.2	0.3	1.15	0.02	1.18	0.68	2	5	6	-0.23	0.03	-0.12	0.02	46.21	0.914	5.40[d]
BZ-117L	13.5	Harzburgite	1	2	2	3.5	0.0	0.86	0.04	1.04	0.19	1	1	1	-0.21		-0.12		45.46	0.914	21.0
BZ-131L	19.2	Harzburgite	2	3	3	3.6	0.5	1.20	0.07	1.17	0.42	1	2	3	-0.19	0.04	-0.10	0.03	45.88	0.913	14.1[d]
BZ-216	23.2	Harzburgite	1	2	2	0.5	0.1	1.43	0.02	1.46	0.10	2	3	5	-0.21	0.04	-0.12	0.01	45.90	0.915	65.0
BZ-201L	23.5	Lherzolite	2	3	3	1.6	0.1	1.37	0.03	1.38	0.48	2	3	5	-0.25	0.02	-0.13	0.01	44.60	0.909	77.0
BZ-203L	23.9	Lherzolite	2	3	3	3.7	0.9	1.17	0.07	1.29	0.28	2	3	4	-0.24	0.09	-0.12	0.04	44.36	0.909	62.0
BZ-120	26.8	Lherzolite				4.5		1.12	0.03			1	2	2	-0.25	0.06	-0.14	0.03	42.65	0.906	35.0
BZ-134L	39.9	Lherzolite	1	1	1	3.7	0.0	1.15	0.07	1.02		3	3	5	-0.24	0.07	-0.13	0.04	44.43	0.913	5.00
BZ-143	72.3	Lherzolite	1	2	2	3.8		1.41	0.08	1.44		3	3	6	-0.20	0.10	-0.10	0.05	42.24	0.905	8.00
BZ-145	79.0	Lherzolite				4.8		1.09	0.03			1	2	2	-0.27	0.06	-0.14	0.01	41.97	0.904	8.48[d]
BZ-146	83.3	Plag Lher	2	2	2	1.5	0.2	1.35	0.05	1.19	0.43	2	4	5	-0.25	0.04	-0.13	0.02	41.60	0.905	16.0
BZ-250	84.3	Plag Lher	2	2	2	1.3	0.7	1.36	0.01	1.46	0.31	2	3	4	-0.25	0.08	-0.12	0.06	40.39	0.904	20.0
BZ-251	86.2	Plag Lher	1	2	2	3.6	0.1	1.39	0.05	1.46	0.20	3	3	5	-0.24	0.01	-0.12	0.01	39.43	0.899	35.0
BZ-252	87.9	Plag Lher	1	1	1	3.3	0.0	1.48	0.09	1.26		2	2	4	-0.25	0.04	-0.13	0.03	38.70	0.895	56.0
BZ-253	89.3	Plag Lher	2	2	2	-0.2	0.3	1.64	0.05	1.55	0.33	1	2	3	-0.21	0.03	-0.11	0.02	40.06	0.907	113
BZ-254	94.7	Plag Lher	1	1	1	2.0	0.0	1.56	0.07	1.48	0.34	1	3	5	-0.23	0.03	-0.12	0.03	40.18	0.900	70.0

[a] The Li concentrations were determined by isotope dilution method.

[b] The Li concentrations were obtained by peak height comparison with L-SVEC.

[c] The La concentrations are from Takazawa et al. (2000).

[d] From Takazawa et al. (unpublished data).

Table 2

Table 2 Lithium and magnesium isotopic compositions of mineral separates in Horoman peridotite massif

Sample ID	Mineral mode (%)	δ^{26}Mg (‰)	2SD	δ^{25}Mg (‰)	2SD	δ^{7}Li (‰)	2SD	[Li] (μg/g)
BZ-216 ol	77.2	-0.23	0.01	-0.12	0.02	0.4		1.48
BZ-216 cpx	3.0	-0.13		-0.07		0.6		1.30
BZ-216 opx	19.6	-0.24	0.04	-0.12	0.02	1.1		0.90
BZ-216 WR^{C}		-0.23		-0.12		0.5		1.36
BZ-216 WR^{M}		-0.21	0.04	-0.12	0.01	0.5	0.1	1.43
BZ-250 ol	62.1	-0.29	0.03	-0.15	0.00	0.7		1.60
BZ-250 cpx	8.0	-0.21	0.03	-0.10	0.03	2.1		1.85
BZ-250 opx	25.3	-0.28	0.04	-0.15	0.02	3.4		1.03
BZ-250 WR^{C}		-0.27		-0.14		1.5		1.40
BZ-250 WR^{M}		-0.25	-0.25	-0.12	0.06	1.3	0.7	1.36

^{C}: Calculated bulk δ^{26}Mg based on mineral mode from Takazawa et al. (2000)
^{M}: Measured bulk δ^{26}Mg

Table 3

Table 3 Parameters for diffusion in a sphere model

	C_1 (μg/g)[a]	Kd	C_0 (μg/g)[e]	D at 1200 °C (m^2/s)[f]	D at 950 °C (m^2/s)[f]	Grain Radius (mm)
melt	11.1 - 12.5[b]					
ol	1.2	0.15[c]	1.67 - 1.88	2.9×10^{-15}	3.8×10^{-17}	1.5
cpx	0.7	0.09[d]	0.96 - 1.08	2.1×10^{-11}	2.8×10^{-13}	0.1

[a]: the initial Li concentration in the melt or in mineral of interest, which is calculated by the Li concentration in bulk unmetasomatised peridotites and the inter-mineral partition coefficients (Brenan et al., 1998; Ottolini et al., 2009; Yakob et al., 2012)
[b]: calculated by 0.1-2% batch melting from a primitive mantle source
[c]: from Brenan et al. (1998)
[d]: calculated based on $Kd^{ol/melt}$ (Brenan et al., 1998) and $Kd^{ol/clinopyroxene}$ (Ottolini et al., 2009; Yakob et al., 2012)
[e]: calculated by the concentration of the melt and the Kd
[f]: Li diffusivities in olivine and clinopyroxene at 1200 and 950 ℃ calculated by using equation (20) in Dohmen et al. (2010) and Coogan et al. (2005)

In addition to those already described above, we assume the initial δ^7Li value in melt is ~3.5 ‰ based on the pristine Li isotopic composition in the upper mantle (e.g. Pogge von Strandmann et al 2011). Melts generated from the equilibrium mantle melting should have a similar δ^7Li value to their source (Jeffcoate et al., 2007) and typically show little variability around this value (see Krienitz et al. 2012). The initial δ^7Li value is set to be ~3.5 ‰ for olivine, as this dominates the bulk peridotite composition. We further briefly consider diffusive exchange with clinopyroxene, which for convenience we assume has the same δ^7Li as olivine.

Figure 1

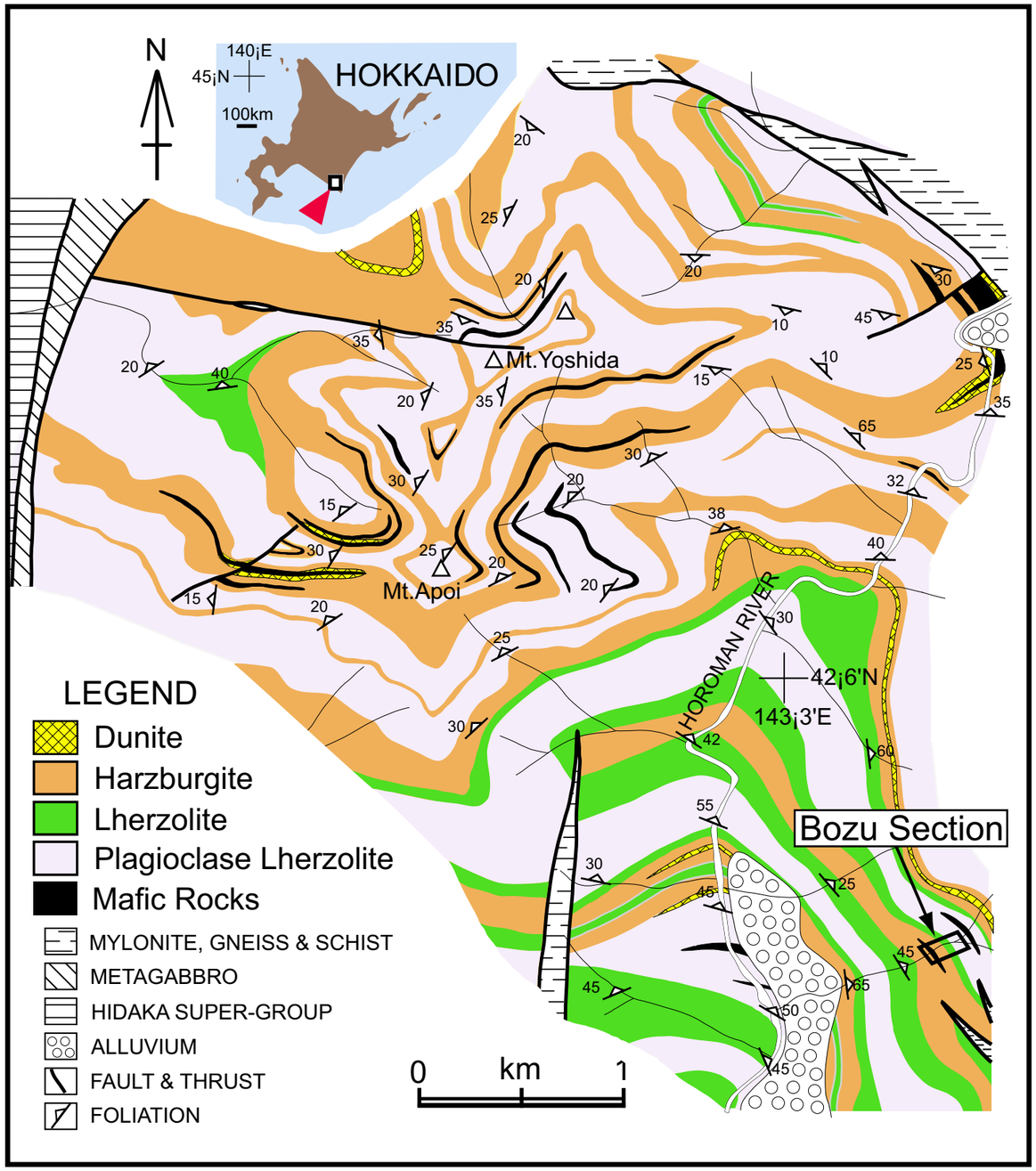
N
140¡E
45¡N
HOKKAIDO
100km
Mt.Yoshida
Mt.Apoi
HOROMAN RIVER
42¡6'N
143¡3'E
Bozu Section
LEGEND
Dunite
Harzburgite
Lherzolite
Plagioclase Lherzolite
Mafic Rocks
MYLONITE, GNEISS & SCHIST
METAGABBRO
HIDAKA SUPER-GROUP
ALLUVIUM
FAULT & THRUST
FOLIATION
0 km 1

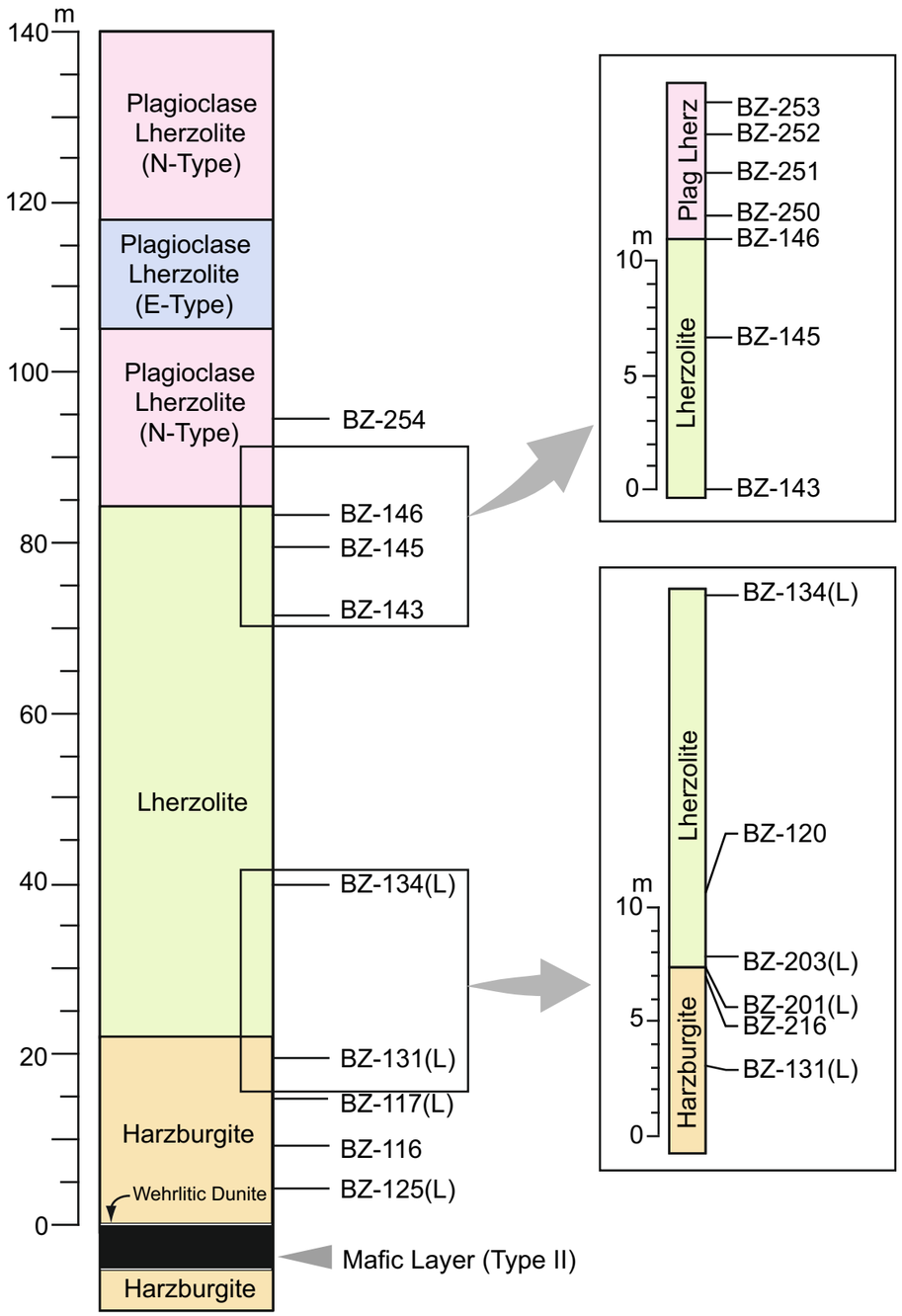
m
140
120
100
80
60
40
20
0
Plagioclase Lherzolite (N-Type)
Plagioclase Lherzolite (E-Type)
Plagioclase Lherzolite (N-Type)
Lherzolite
Harzburgite
Wehrlitic Dunite
Harzburgite
BZ-254
BZ-146
BZ-145
BZ-143
BZ-134(L)
BZ-131(L)
BZ-117(L)
BZ-116
BZ-125(L)
Mafic Layer (Type II)
Plag Lherz
Lherzolite
BZ-253
BZ-252
BZ-251
BZ-250
BZ-146
BZ-145
BZ-143
BZ-134(L)
Lherzolite
Harzburgite
BZ-120
BZ-203(L)
BZ-201(L)
BZ-216
BZ-131(L)

Figure 2

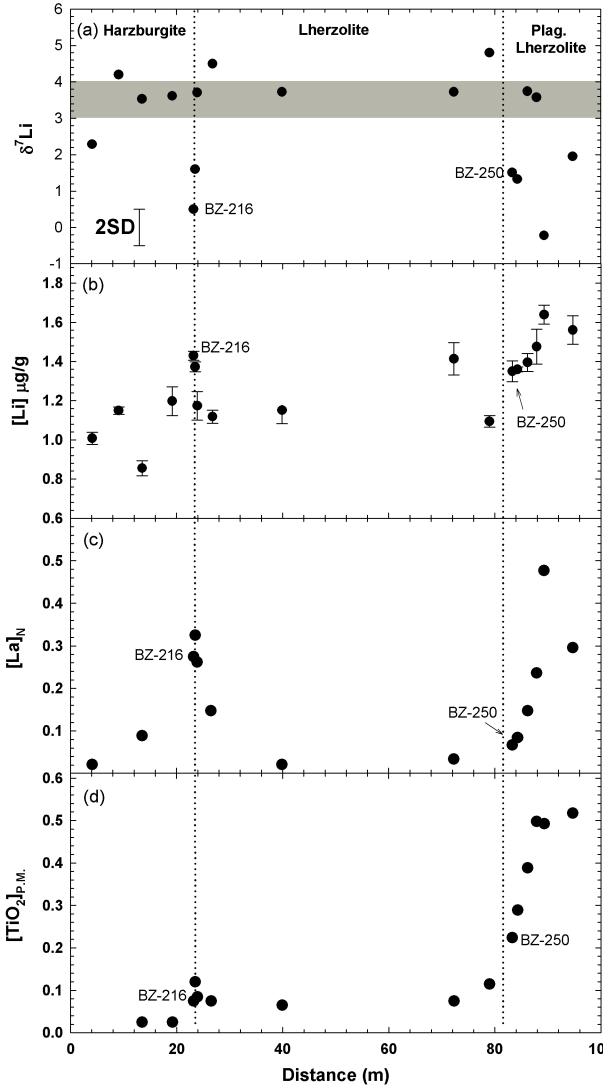
(a) Harzburgite
Lherzolite
Plag. Lherzolite
δ7Li
2SD
BZ-216
BZ-250
(b)
[Li] μg/g
BZ-216
BZ-250
(c)
[La]N
BZ-216
BZ-250
(d)
[TiO2]P.M.
BZ-216
BZ-250
Distance (m)

Figure 3

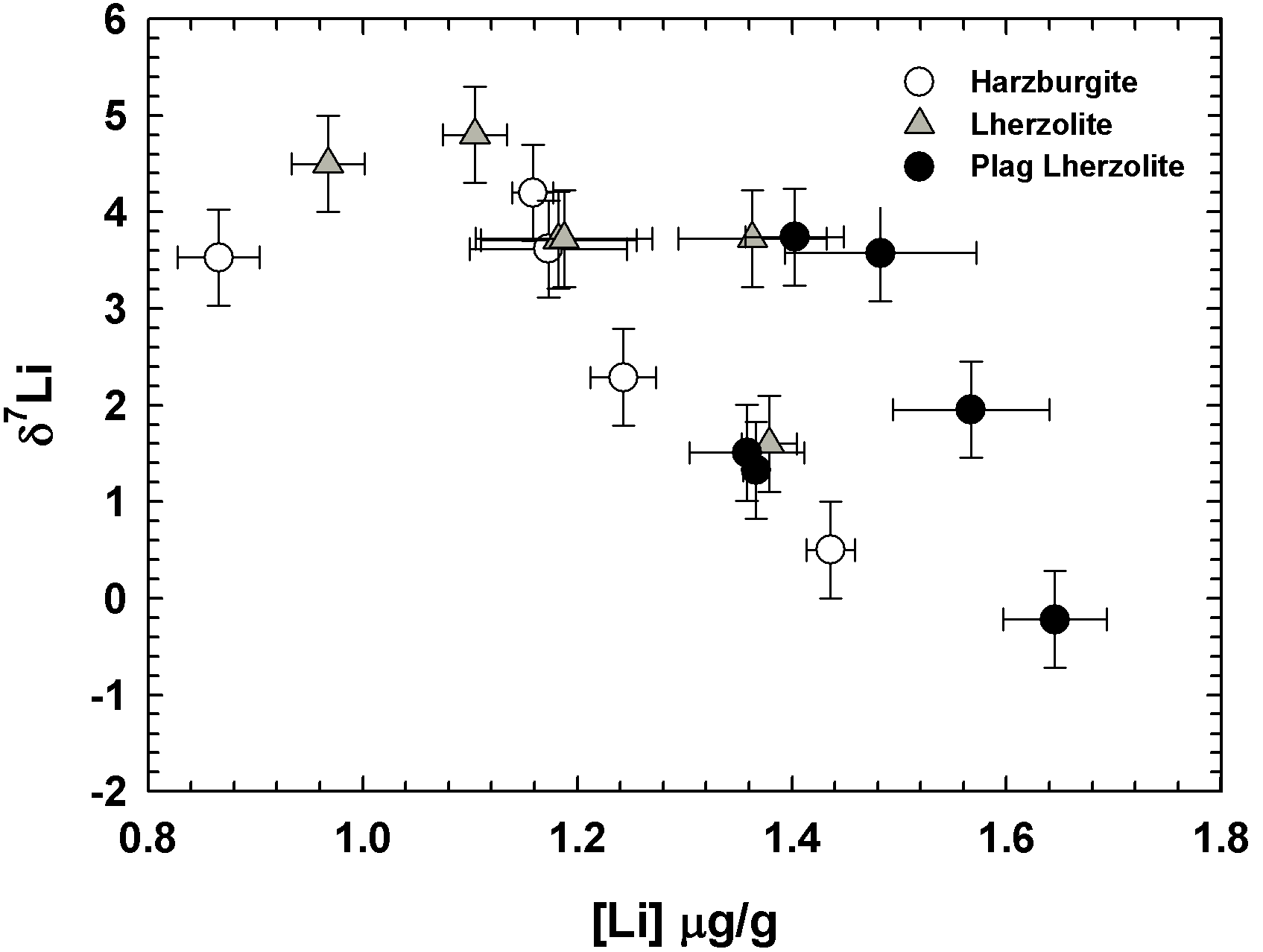
Harzburgite
Lherzolite
Plag Lherzolite
δ7Li
[Li] μg/g
6
5
4
3
2
1
0
-1
-2
0.8
1.0
1.2
1.4
1.6
1.8

Figure 4

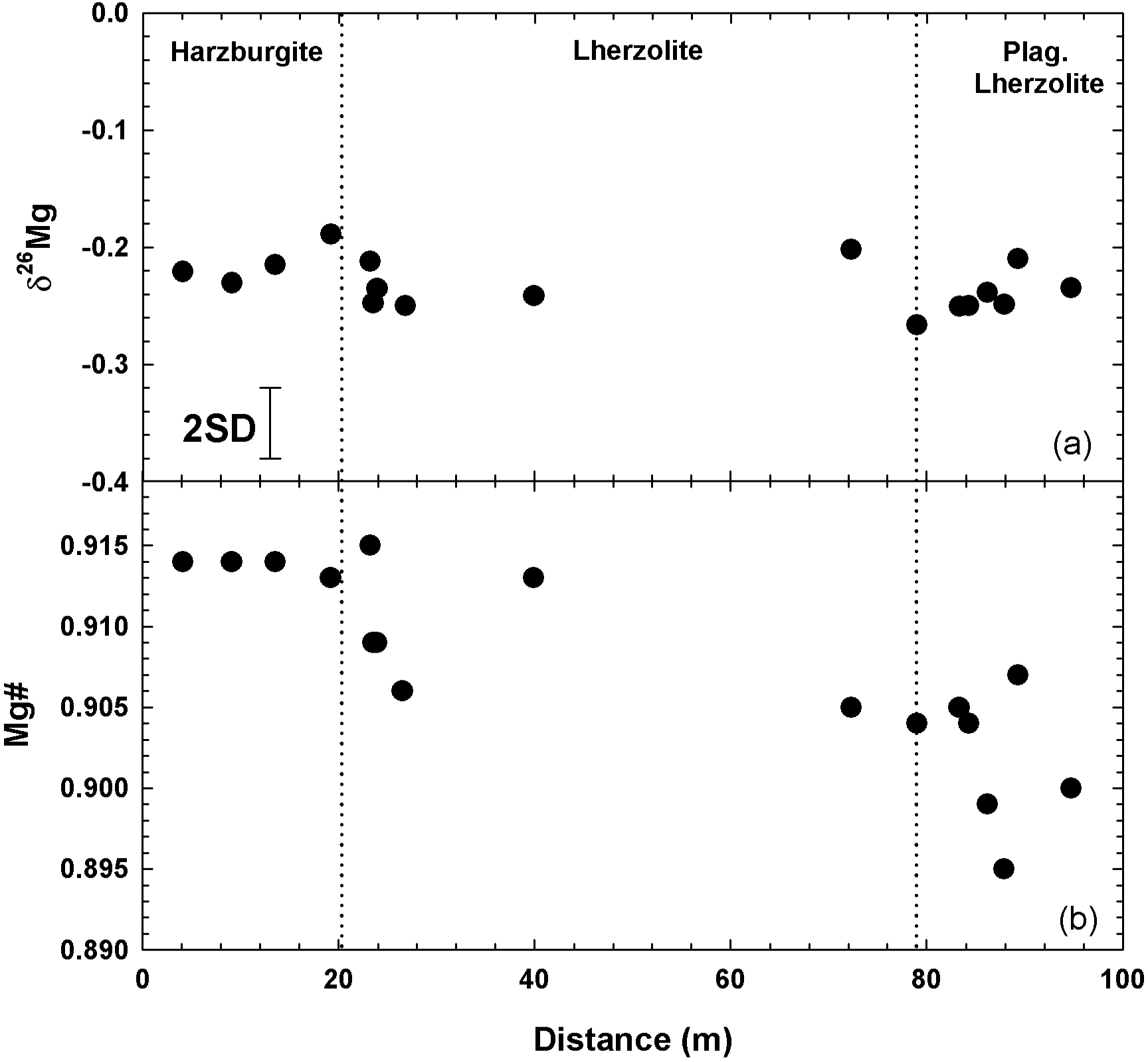
Harzburgite
Lherzolite
Plag. Lherzolite
δ^{26}Mg
2SD
(a)
Mg#
(b)
Distance (m)
0.0
-0.1
-0.2
-0.3
-0.4
0.915
0.910
0.905
0.900
0.895
0.890
0
20
40
60
80
100

Figure 5

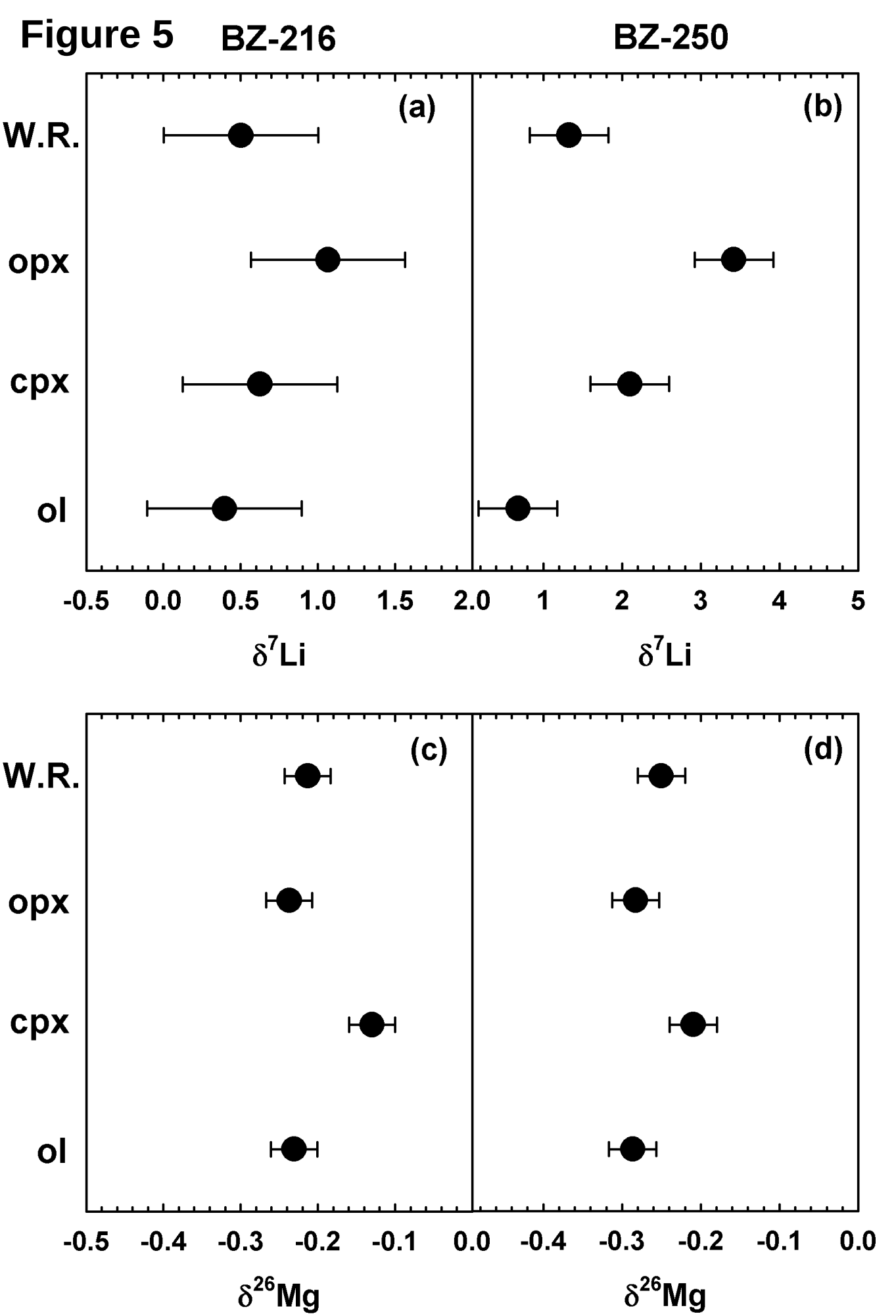
BZ-216
BZ-250
(a)
(b)
(c)
(d)
W.R.
opx
cpx
ol
-0.5
0.0
0.5
1.0
1.5
2.0
1
2
3
4
5
δ7Li
δ7Li
-0.5
-0.4
-0.3
-0.2
-0.1
0.0
-0.4
-0.3
-0.2
-0.1
0.0
δ26Mg
δ26Mg

Figure 6

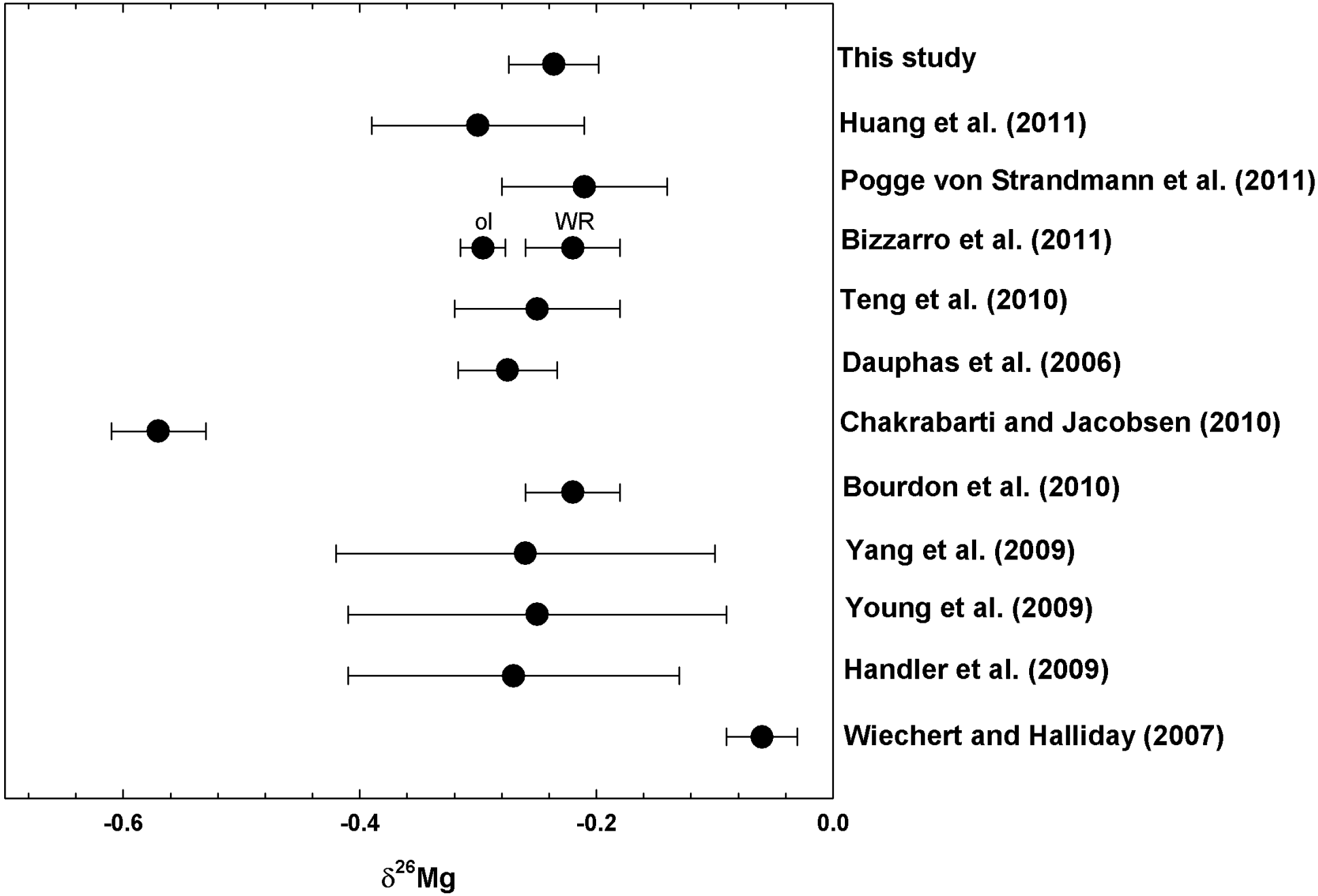
This study
Huang et al. (2011)
Pogge von Strandmann et al. (2011)
ol
WR
Bizzarro et al. (2011)
Teng et al. (2010)
Dauphas et al. (2006)
Chakrabarti and Jacobsen (2010)
Bourdon et al. (2010)
Yang et al. (2009)
Young et al. (2009)
Handler et al. (2009)
Wiechert and Halliday (2007)
-0.6
-0.4
-0.2
0.0
δ26Mg

Figure 7

(a) Initial status of the mantle

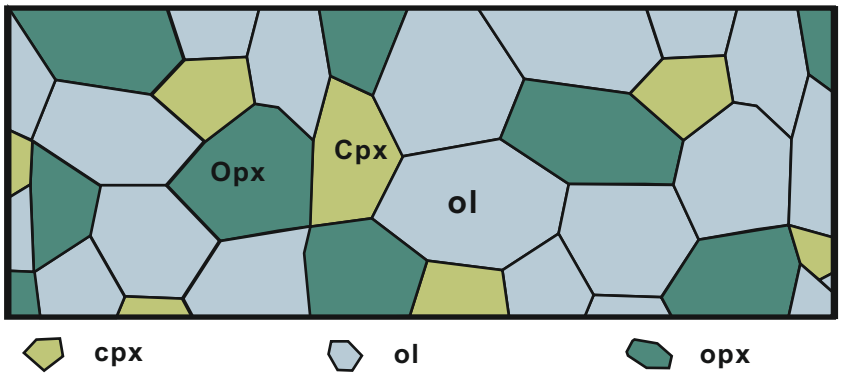

(b) Li diffusion from melt to crystals

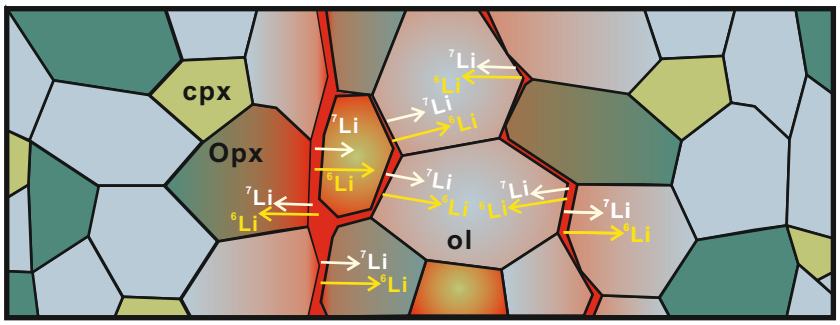

(c) Diffusion of Li from enriched zone into country rock

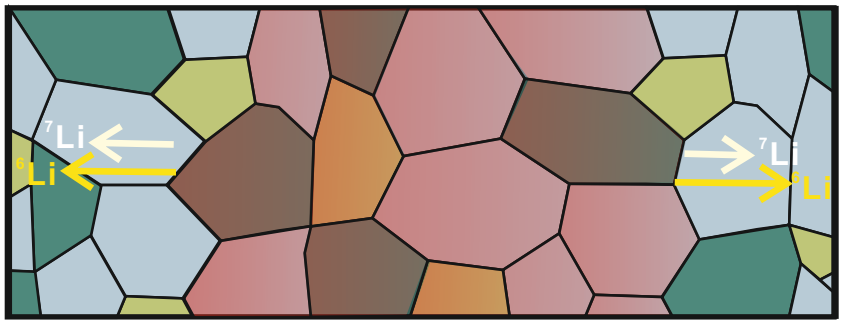

Figure 8

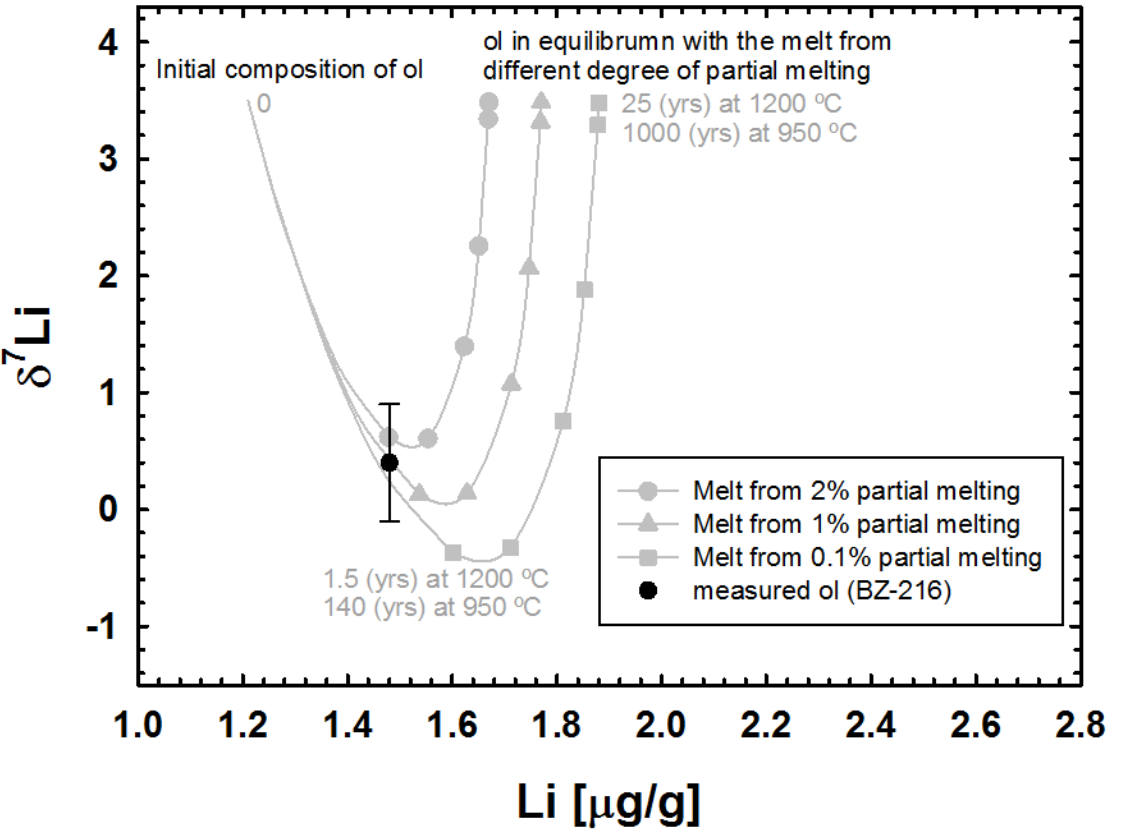
Initial composition of ol
0
ol in equilibrumn with the melt from
different degree of partial melting
25 (yrs) at 1200 °C
1000 (yrs) at 950 °C
1.5 (yrs) at 1200 °C
140 (yrs) at 950 °C
Melt from 2% partial melting
Melt from 1% partial melting
Melt from 0.1% partial melting
measured ol (BZ-216)
δ7Li
Li [μg/g]
4
3
2
1
0
-1
1.0
1.2
1.4
1.6
1.8
2.0
2.2
2.4
2.6
2.8

Figure 9

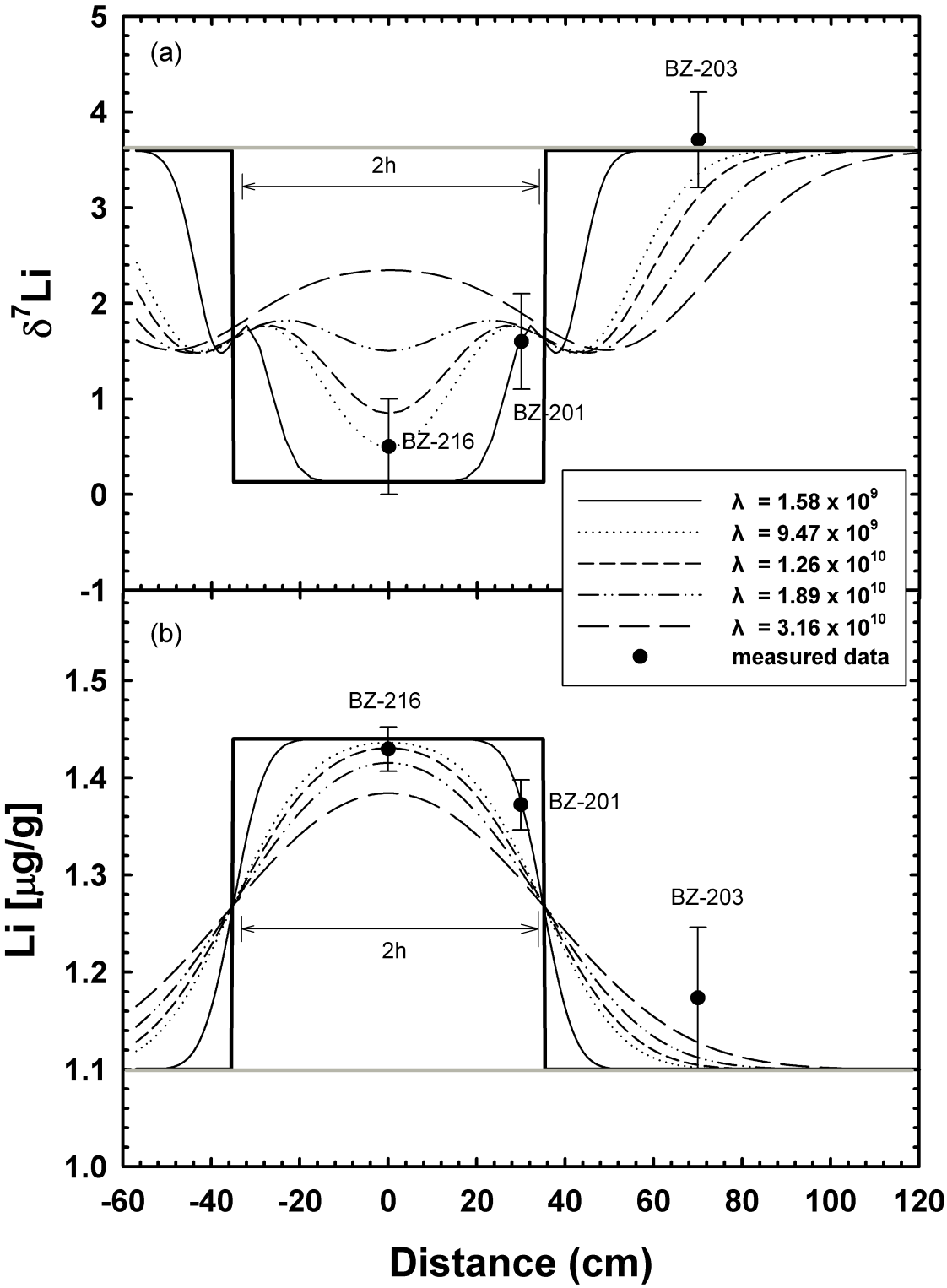
(a)
BZ-203
2h
BZ-201
BZ-216
δ^7Li
λ = 1.58 x 10^9
λ = 9.47 x 10^9
λ = 1.26 x 10^10
λ = 1.89 x 10^10
λ = 3.16 x 10^10
measured data
(b)
BZ-216
BZ-201
BZ-203
2h
Li [μg/g]
Distance (cm)